Tectonophysics 670 (2016) 82–100

Contents lists available at ScienceDirect

Tectonophysics

journal homepage: www.elsevier.com/locate/tecto

Earthquake relocation using a 3D a-priori geological velocity model from the western Alps to Corsica: Implication for seismic hazard

Nicole Béthoux [a,*], Thomas Theunissen [b], Marie-Odile Beslier [a], Yvonne Font [a], François Thouvenot [c], Jean-Xavier Dessa [a], Soazig Simon [a], Gabriel Courrioux [d], Antonio Guillen [d]

[a] University of Nice — Sophia Antipolis, UMR 6526-Geoazur, UNS-CNRS-IRD-UPMC, 250 rue Albert Einstein, Sophia-Antipolis, 06560, Valbonne, France
[b] University of Bergen, Department of Earth Science, Allegaten, 41, 5020, Bergen, Norway
[c] Institut des Sciences de la Terre, University of Grenoble/CNRS, BP 53, 38041 Grenoble Cedex 9, France
[d] BRGM, BP 6000, 45060 Orléans Cedex 2, France

ARTICLE INFO

Article history:
Received 14 May 2015
Received in revised form 30 November 2015
Accepted 23 December 2015
Available online 4 January 2016

Keywords:
3-D modelling of crustal geometry
3-D earthquake location
Alps and Ligurian Sea
Active tectonics

ABSTRACT

The region between the inner zones of the Alps and Corsica juxtaposes an overthickened crust to an oceanic domain, which makes difficult to ascertain the focal depth of seismic events using routine location codes and average 1D velocity models. The aim of this article is to show that, even with a rather lose monitoring network, accurate routine locations can be achieved by using realistic 3D modelling and advanced location techniques. Previous earthquake tomography studies cover the whole region with spatial resolutions of several tens of kilometres on land, but they fail to resolve the marine domain due to the absence of station coverage and sparse seismicity. To overcome these limitations, we first construct a 3D a-priori P and S velocity model integrating known geophysical and geological information. Significant progress has been achieved in the 3D numerical modelling of complex geological structures by the development of dedicated softwares (e.g. 3D GeoModeller), capable at once of elaborating a 3D structural model from geological and geophysical constraints and, possibly, of refining it by inversion processes (Calcagno et al., 2008). Then, we build an arrival-time catalogue of 1500 events recorded from 2000 to 2011. Hypocentres are then located in this model using a numerical code based on the maximum intersection method (Font et al., 2004), updated by Theunissen et al. (2012), as well as another 3D location technique, the NonLinLoc software (Lomax and Curtis, 2001). The reduction of arrival-time residuals and uncertainties (dh, dz) with respect to classical 1D locations demonstrates the improved accuracy allowed by our approach and confirms the coherence of the 3D geological model built and used in this study. Our results are also compared with previous works that benefitted from the installation of dense temporary networks surrounding the studied epicentre area.

The resulting 3D location catalogue allows us to improve the regional seismic hazard assessment, more particularly in the south of the Argentera massif and in the Ligurian basin.

1. Introduction

The south-western Alps and the northern part of the Ligurian basin (western Mediterranean Sea) and the very populated littoral French and Italian Rivieras inbetween, are prone to frequent earthquakes of low to moderate magnitudes. The strong structural heterogeneity of the region—from the core of the Alps to Corsica through an oceanic domain (Figs. 1 and 2)—complicates the determination of earthquake focal depths using routine location codes and average 1D velocity models. The aim of this study is to improve earthquake locations in the area by computing more precisely the geometry of seismic rays (and therefore the corresponding travel times) between earthquakes and seismic stations.

Several recent tomographic studies helpfully refined our knowledge of lithospheric 3D P-wave velocity structures in the Alps and the neighbouring Italian peninsula (Diehl et al., 2009; Scafidi et al., 2009; Di Stefano et al., 2009). However, because these tomographic models cover large regions, their spatial resolutions are generally limited to several tens of kilometres; they are neither well resolved in the marine domain, due to poor or even absent coverage of these seismogenic areas. Conversely, the Ligurian basin and the northern Tyrrhenian Sea have been investigated through several seismic cruises which provided some insight into crustal structures and velocity distributions.

To address these issues, our strategy is to build an a-priori 3D structural model integrating known geophysical and geological information. We used a geological modelling tool ('3D Geomodeller') developed by the 'Bureau de Recherches Géologiques et Minières' (BRGM) and licenced by 'Intrepid Geophysics' to define the 3D geometry of the main interfaces defining the large-scale structure in the study area,

* Corresponding author.
E-mail address: bethoux@geoazur.unice.fr (N. Béthoux).

http://dx.doi.org/10.1016/j.tecto.2015.12.016
0040-1951/

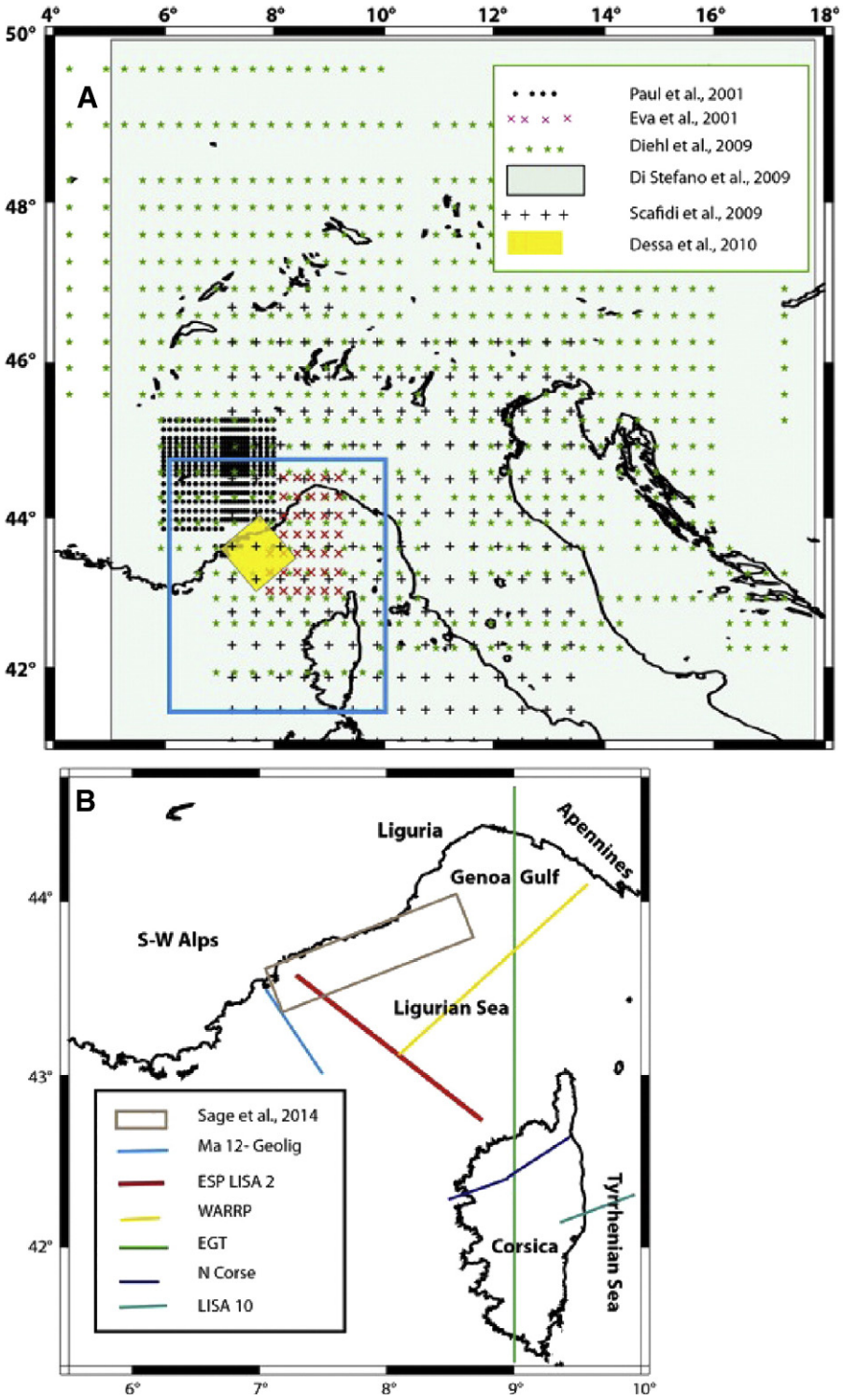

Fig. 1. a. Location of the study. Sets of dots represent the tomography grids (Paul et al., 2001; Eva et al., 2001; Diehl et al., 2009; Di Stefano et al., 2009; Scafidi et al., 2009) that are introduced in the 3D model. The limits of the model are framed by a rectangle. b. Location of the main seismic lines or active tomography grids used for the geological model (LISA campaign: Contrucci et al., 2001; Contrucci et al., 2005; MALIS campaign: Rollet et al., 2002; ESP: Le Douaran et al., 1984; WRRP: Wide Aperture reflection and refraction Profile, Makris et al., 1999; EGT: Egger et al., 1988; N Corse: Béthoux et al., 1999; Geolig: Operto (pers comm); Sage et al., 2011; Dessa et al., 2011).

which includes sedimentary and crustal layers (both continental and oceanic) together with a Moho geometry of this complex zone. We then introduced in this structural model P and S velocities borrowed from a synthesis of both active source and passive tomographic inversions. The adequacy of this model is tested a posteriori from its ability to provide improved event locations which agree with the position of active known or suspected faults. The results allow to discuss the relevance of such a method in the area, and more generally in complex geodynamical regions, and geodynamic and seismic hazards implications.

Since the beginning of instrumental seismology, earthquakes have been regularly recorded along the Ligurian coast some of them widely felt by the population. Major destructive historical ruptures are also known in the same region (Larroque et al., 2001). The 1887 Ligurian

event produced more than 600 fatalities, numerous injuries and a lot of damage. This event was recently revised (Larroque et al., 2012), and the modelling of tsunami waves induced by this offshore earthquake suggests an Mw magnitude reaching 6.8. Historical catalogues also list several destructive earthquakes in the south of the Argentera massif, an area where instrumental catalogues only provide microseismicity data, with diffuse epicentres (Bauve et al., 2014). More particularly, the location of the 1564 Nissart earthquake (Lambert and Levret, 1996; Scotti et al., 2007) remains very enigmatic.

Instrumental seismicity is generally characterized by diffuse microseismicity as in the southernmost part of the western Alps. However, some events of magnitude > 4 used to occur, widely felt by the population and even provoking few damages, as in the Ubaye area, north of our studied region and along the northern Ligurian coast, east off Nice, up to the centre of the basin as the 1963/07/19 event that reached the magnitude 6, happily located around 80 km off the coast.

Precise epicentre location is therefore a key element to improve our knowledge of historical and strong instrumental earthquakes allowing us to image the geometry of active faults and to precise the seismogenic depth. Taking into account the occurrence of such events, it is important to define a methodology to reach a good precision of seismic location. Previous works benefited from the installation of dense temporary networks covering limited areas (Eva et al., 2001; Paul et al., 2001; Courboulex et al., 2007; Turino et al., 2009; Dessa et al., 2011). We show here that, instead of installing dense networks for a short period of time, we can provide routine accurate locations if we use a realistic 3D medium and if we improve the location technique.

2. Geodynamical and geological settings

Our study area covers, from south to north, Corsica, the Ligurian basin, the north-western part of the Tyrrhenian Sea, the Ligurian coast, the coast along the northern Apennines, and the south-western Alps, including the Argentera massif (Fig. 1). The region is therefore characterized by a complex geological setting.

The evolution of the southern part of the western Alpine arc is characterized by several deformation phases since the Oligocene (Tricart et al., 2006). From the Neogene onwards, the tectonic evolution of the western Alps was driven by large dextral strike-slip fault systems in the inner Alps, which accommodated the oblique indentation of the Adria microplate (i.e. 'Insubric Line', Vialon et al., 1989), combined to thrust motions in the external part. A transition from transpressional to transtensional regimes was dated at 8–5 Ma in the Ubaye zone (Sanchez et al., 2010). A transpressional regime is also recognized in the Ligurian Alps to the east (Bauve et al., 2014). In the meantime, the Mesozoic to Cenozoic sedimentary cover previously deformed during the E–W compression phase was subjected to a N–S shortening during the Miocene. This style of deformation was still active during the Pliocene as suggested by dextral strike-slip reactivation of thrust faults in the foreland sedimentary cover (Courboulex et al., 2007) and by the uplift of the northern Ligurian margin Bigot- et al., 2004; Sage et al., 2011). This rifted margin is singular in that it lies immediately next to the Alpine orogenic arc. It was formed in the general context of convergence between the African and Eurasian plates that underwent the subduction of the Tethys Ocean, the collision and accretion of continental blocks of the Tethyan plate—locally responsible for the Alpine and Apennine orogenies—some back-arc rifting and oceanic spreading. The Ligurian basin opened in response to the anticlockwise rotation of the Corsican–Sardinian block during the Lower Miocene; it was preceded by an Oligocene rifting phase (Réhault et al., 1984; Speranza and Chiappini, 2002) that occurred within the Alpine-Northern Apennine collision belt and therefore presumably affected an initially thick crustal continental domain in the Ligurian region. The major known structures of the basin and its margins are inherited from the rifting phase and spreading. However the basin is reactivated in compression, as attested by the instrumental seismicity (Béthoux et al., 2008), the geometry of the active faults remaining not well defined. Nowadays GPS measurements attest to very low strain rate in the south-western Alps–Ligurian basin area (Nocquet and Calais, 2003; Larroque et al., 2009).

3. Building the 3D a priori model

3.1. Constructing the structural model

The structural model is constructed in a volume delimited between latitudes 41.3°N and 44.7°N, longitudes 6°E and 10.2°E (Fig. 1b) and from the surface topography to 80 km depth, that is to say a volume of 300 km × 200 km × 83 km. In this region, the Moho depth varies from 12 km under the Ligurian basin up to 55 km under the north of the Argentera massif. The thickness of the sedimentary covers also widely varies from one area to another reaching 8 km in the Ligurian basin. Three types of crust nature and/or rheology are evidenced in the region (oceanic, transitional and continental, Fig. 2).

The model is based on a bibliographic review of all structural and velocity information available in the region resulting from partial explorations by different scientific teams and with different techniques since the 70s. A main difficulty of this work consisted in ensuring the coherency between those multiple datasets. Several tomographic studies are available for the western Alps (Fig. 1a), while, for Corsica and the Ligurian basin, the data mainly consists in a series of 2D seismic profiles (Fig. 1b). In the western Alps, we carefully checked the compatibility between the solutions from different tomographic models in the same geographic area. In the south, we have to weight and interpolate data of different quality and of heterogeneous spatial repartition.

In the following, we present the available data and explain how we built the model and which interpolation techniques were used. The objective is to get the best compromise between data accuracy, pertinent simplification and interpolation, and model size. We consider 5 main geological interfaces at crustal scale, which is obviously a simplification of the geological structures. Those interfaces are: (1) the topography/bathymetry surface, (2) the sedimentary/basement interface, (3) the Moho, (4) the boundary of the Ivrea body under the internal part of the Alps, and (5) an intermediate crustal layer existing under the deep continental margins in the northeastern end of the Ligurian basin and characterized by an average velocity Vp = ±7.2–7.3 km/s (Makris et al., 1999; Contrucci et al., 2001). Two of these interfaces, the oceanic intermediate crust and the Ivrea body, are locally limited whereas the three others are continuous within the whole model.

These interfaces mainly result from indirect geophysical data and might not have a strict geological meaning. They are in most cases defined by seismic velocity transitions evidenced by earthquake tomography, or by strong reflectors in seismic profiles.

1) The topography/bathymetry interface

This is the upper boundary of the model, overlaid with air or water. The DEM is based on a compilation of marine data and of French and Italian satellite data. The inland French data are defined with a resolution of 50 m and the Italian ones of 90 m. These data have been decimated/interpolated at a step of 500 m and introduced in '3D Geomodeller'.

2) The top of the crust

This interface defines the base of the sedimentary layer. It was constructed differently inland and offshore.

Inland, the interface geometry was first borrowed from geological data. The boundaries of the crystalline massifs in the mainland (Argentera and Maures-Esterel) and in Corsica were derived from geological maps at a 1/250,000 scale. Elsewhere, the thickness of the sedimentary thickness was estimated from balanced geological cross-sections as in the Nice Arc (Schreiber et al., 2010) or the Castellane Arc (Laurent et al., 2000). The thickness of the sedimentary layer was also derived from local earthquake tomography studies (Paul et al., 2001; Eva et al., 2001; Diehl et al., 2009; Scafidi et al., 2009; Turino et al., 2009; Di Stefano et al., 2009).

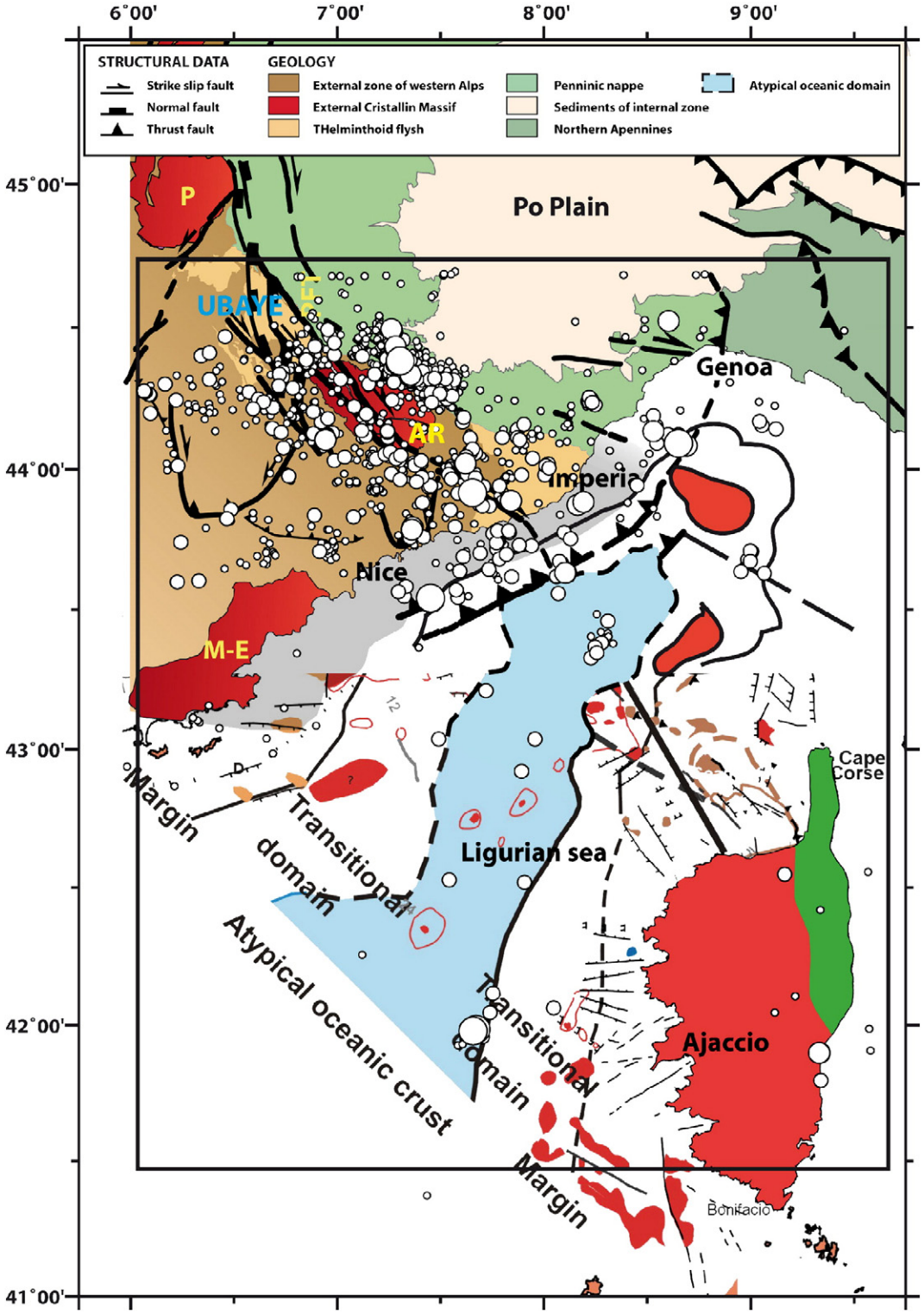

Fig. 2. Geological framework of the region, modified from Bauve et al. (2014) for the northern part and from Rollet et al. (2002) for the southern part. The seismicity (obtained with the 3D model) is superimposed, as well as the limits of the 3D velocity model.

For the marine domain, numerous vertical seismic profiles are available, mainly for the northern continental margin of the Ligurian Sea (Réhault et al., 1984; Contrucci et al., 2001; Rollet, 1999; Rollet et al., 2002; Sage et al., 2011). In each profile, we digitized the reflector interpreted as the top of the crust and converted the two-way travel-time to depth by using a Vp law inferred from wide-angle seismic data analysis (Contrucci et al., 2001; Rollet, 1999; Rollet et al., 2002; Dessa et al., 2011).

3) The marine crustal intermediate layer

This layer is evidenced in most of the 2D wide-angle seismic profiles acquired in the Liguro-Provençal Basin (Ansorge et al., 1992; Pascal et al., 1993; Makris et al., 1999; Rollet, 1999; Rollet et al., 2002; Contrucci et al., 2001; Gailler et al., 2009; Dessa et al., 2011). It is 1 to 3 km thick and characterized by P-wave velocities ranging from 7.2 to 7.8 km/s. It overlay the Moho at the foot of the two conjugate margins and in the northeastern end of the basin. Its geometry is not well

resolved but it disappears in the central part of the basin and seems to be tapered under its margins. We extended the geometry of this layer, seemingly present in all the Ligurian Sea and beyond, from the sparse available data. This layer is about 2-km thick at the foot of the northern margin and in the gulf of Genoa, under the thin continental crust of the North Tyrrhenian Sea, and about 3-km thick at the foot of the Corsican margin.

4) The boundaries of the Ivrea body

The Ivrea body, responsible to a very strong Bouguer anomaly in the western Alps, is formed of a slice of high-density and high-seismic-velocity material interpreted as a wedge of anomalous upper mantle in the European crust. The lateral geometry of the Ivrea body was determined by a gravimetric inversion carried out by Schreiber et al. (2010) using '3D Geomodeller'.

5) The Mohorovicic interface

Three types of data are available to constrain the Moho interface:

- The Moho deduced from gravimetric anomaly inversion at the scale of the whole region (Chamot-Rooke et al., 1999) or, more locally, in the southern Alps around the Ivrea Body (Schreiber et al., 2010).
- The Moho depth obtained by 3D tomographic studies (Paul et al., 2001; Eva et al., 2001; Diehl et al., 2009; Scafidi et al., 2009; Dessa et al., 2011). These tomographic results have very different grid resolution, from 350 m up to 50 km. Where models overlap (Fig. 1a), we select the higher-resolution model.
- The Moho resulting from wide-angle seismic campaigns or seismological studies (Hirn and Sapin, 1976; Le Douaran et al., 1984; Ansorge et al., 1992; Waldhauser et al., 1998; Béthoux et al., 1999; Rollet, 1999; Contrucci et al., 2001; Makris et al., 1999; Bertrand and Deschamps, 2000; Thouvenot et al., 2007). However these data are very heterogeneous in acquisition techniques and set ups. Their uneven geographic distributions leave important gaps in the southern border of the Alpine massif and in the southern part of our model (Fig. 1b).

Concerning the continental area (northern part of our model), the comparison of these different kinds of results shows that the gravimetric Moho is generally in good agreement with the Vp = 7.25 km/s isovalue of the tomography model from Diehl et al. (2009). Southward, for the tomography models of the northern Ligurian margin, the gravimetric Moho corresponds to the Vp = 7.70 km/s isovalue of the tomography model from Di Stefano et al. (2009) and to the Vp = 7.5 km/s isovalue from Dessa et al. (2011). Such discrepancies are a direct consequence of variable resolutions of tomographic studies. The gravimetric Moho correctly fits with the Moho depths determined by Béthoux et al. (1999) under Corsica and with those of Ansorge et al. (1992) in the Gulf of Genoa.

By contrast, the depth difference can reach 5 km between this gravimetric Moho and the seismic Moho determined by wide-angle seismic profiles (Le Douaran et al., 1984; Contrucci et al., 2001; Contrucci et al., 2005; Makris et al., 1999), particularly under the margins. Albeit arguably more precisely constrained, we did not take these local values into account and chose to keep the gravimetric Moho in our model because it is homogeneously determined in the whole study area; taking into account isolated local values would have introduced singularities.

The Moho interface is thus defined over a grid with a 2-km step borrowed from the gravity anomaly inversion of Chamot-Rooke et al. (1999). Nevertheless, we modified this interface in two regions: in the complex region of the Ivrea body which benefits from a specific gravimetric inversion (Schreiber et al., 2010), and in the north-eastern part of the model, under the Apennines, where the Vp = 7.25 km/s isovalue corresponding to the tomography performed by Diehl et al. (2009) is 4 to 13 km deeper than the gravimetric Moho: the latter suffers from boundary effects, whereas the tomography is well resolved.

The selected structural interfaces were then digitized into a 3D matrix of voxels in '3D Geomodeller', with blocks of horizontal and vertical dimensions 2 km × 2 km × 0.5 km (see Calcagno et al., 2008 for a thorough description of the procedure). Fig. 3 depicts the 3D model eventually obtained.

3.2. Implementing the P and S velocity model

The geometry and depth of the interfaces built in the model define the top and the base of the main structural layers in which P- and S-wave seismic velocities need to be defined at each node.

Due to geological heterogeneities, the observed P-wave velocities (Vp) deduced from the bibliographic studies that we used to define the interfaces are not constant along these interfaces. We interpolated Vp along one given interface using a «near-neighbour» technique.

The various tomographic grids were kindly provided by their respective authors, as well as the corresponding resolution matrices when available, or resolution tests, in order to proceed only with well-resolved data. However, velocities differ from one model to another, mainly due to variations in the initial 1D reference models used in each inversion (Kissling, 1988) or to different grid steps (velocity values are not homogeneously averaged in pixels of different volumes). In this work, we favour dense grids when available. In addition, the compilation of all tomographic velocities allowed us to construct a vertical linear Vp gradient in each layer, which we could apply in the model as a best guess where no constraining data existed.

Beneath the Moho interface, in the upper mantle, Vp increases to an imposed value of 8.4 km/s at the bottom of the model (80 km), according to the reference iasp91 velocity model.

For S-wave velocities (Vs), we used all the results from the local earthquake tomography studies that provided either Vs grids or Vp/Vs ratios. In the areas where Vp but no Vs values are available, we imposed a Vp/Vs ratio from the rheological characteristics of the medium as described in the literature.

We will discuss in Section 5 how locations are modified when S arrival times are taken into account or not.

Fig. 4 provides examples of cross-sections in the P-velocity model. The N–S first one shows the marked deepening of the Moho from the northern Ligurian margin to the Alps. This interface is globally flat in the oceanic domain with an average depth of 15 km and deepens to 60 km beneath the Alps. The second E–W cross-section, at a latitude of 43.7°N, shows the variation of the crustal thickness from the Maures massif to the Gulf of Genoa. It also shows the thick sedimentary layer beneath the Ligurian basin, a maximum thickness of 5 km being reached at the foot of the north margin. The third E–W cross-section located north

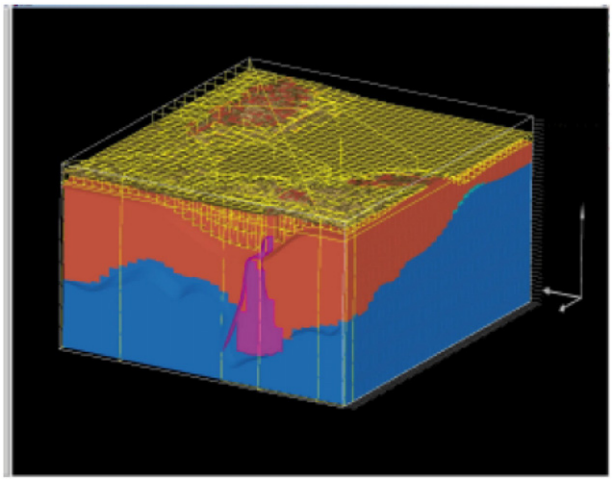

Fig. 3. Representation of the 3D block obtained with the Geomodeller code (see Schreiber et al., 2010 for details). The mesh is represented in yellow at the surface of the block (2 km * 2 km * 1 km). The crust is in red and the mantle in blue. The pink volume is the Ivrea body. The dimensions of the block are 300 km*200 m*83 km.

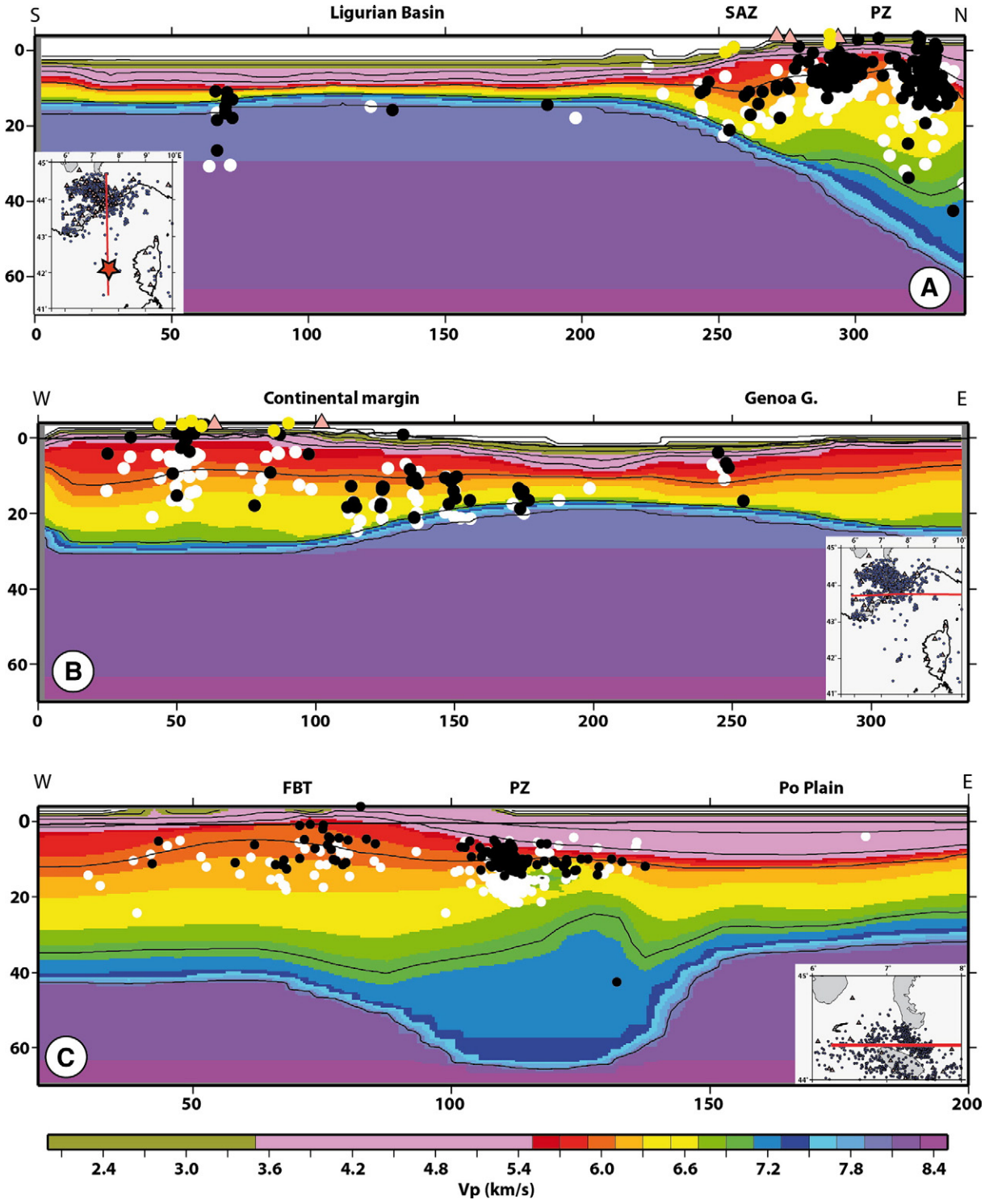

Fig. 4. Sections across the 3D P-velocity model, showing earthquakes located with 1D (white dots) and 3D (black dots) methods. Yellow dots: quarry shots. Earthquakes are projected onto the section if their distance from the section is smaller than 10 km. Location of cross-section shown on the map: a. Cross-section along the 7.2° E longitude. The star in the map shows the location of the 2011 seismic crisis near Corsica. b. Cross-section along the 43.7° N latitude. c. Cross-section along the 44.4°N latitude and zoom of the cross-section corresponding to that described in Paul et al. (2001).

of the Argentera Massif exhibits the crustal root beneath the core of the Alps and also shows the Ivrea body, as a high-velocity anomaly embedded into the crust.

3.3. Wrapping up the model

Finally, to build the velocity grid, we resampled our model using 5 km × 5 km × 2 km cells (horizontal and vertical dimensions respectively), which amounts to a total of 201 000 cells. This model is referenced in UTM coordinates.

Because our study area is large, the flat-Earth approximation yields errors. Therefore, we projected the study volume onto an ellipsoidal Earth. We transformed UTM coordinates into the ellipsoidal WGS84 referential to obtain a new grid in latitudes and longitudes, which provides more accurate geographic coordinates in the region.

4. Seismological data and earthquake location processing

4.1. Catalogue of arrival times

56 regional stations are located in the study area. These stations belong to several French networks, such as RéNaSS (Réseau National de Surveillance Sismique), LDG/CEA (Laboratoire de Détection et de Géophysique du CEA), SISMALP network (Grenoble Observatory), RAP (Réseau Accélérometrique Portable), TRGRS (Nice Observatory) and to RSNI (Regional Seismic Network of North-Western Italy). Fig. 5 shows the seismic station distribution.

We benefited from existing catalogues of arrival times, published by several networks. Because we had to merge these catalogues and read arrival times for several additional stations which had not been previously processed, we restricted the catalogue used in the present study.

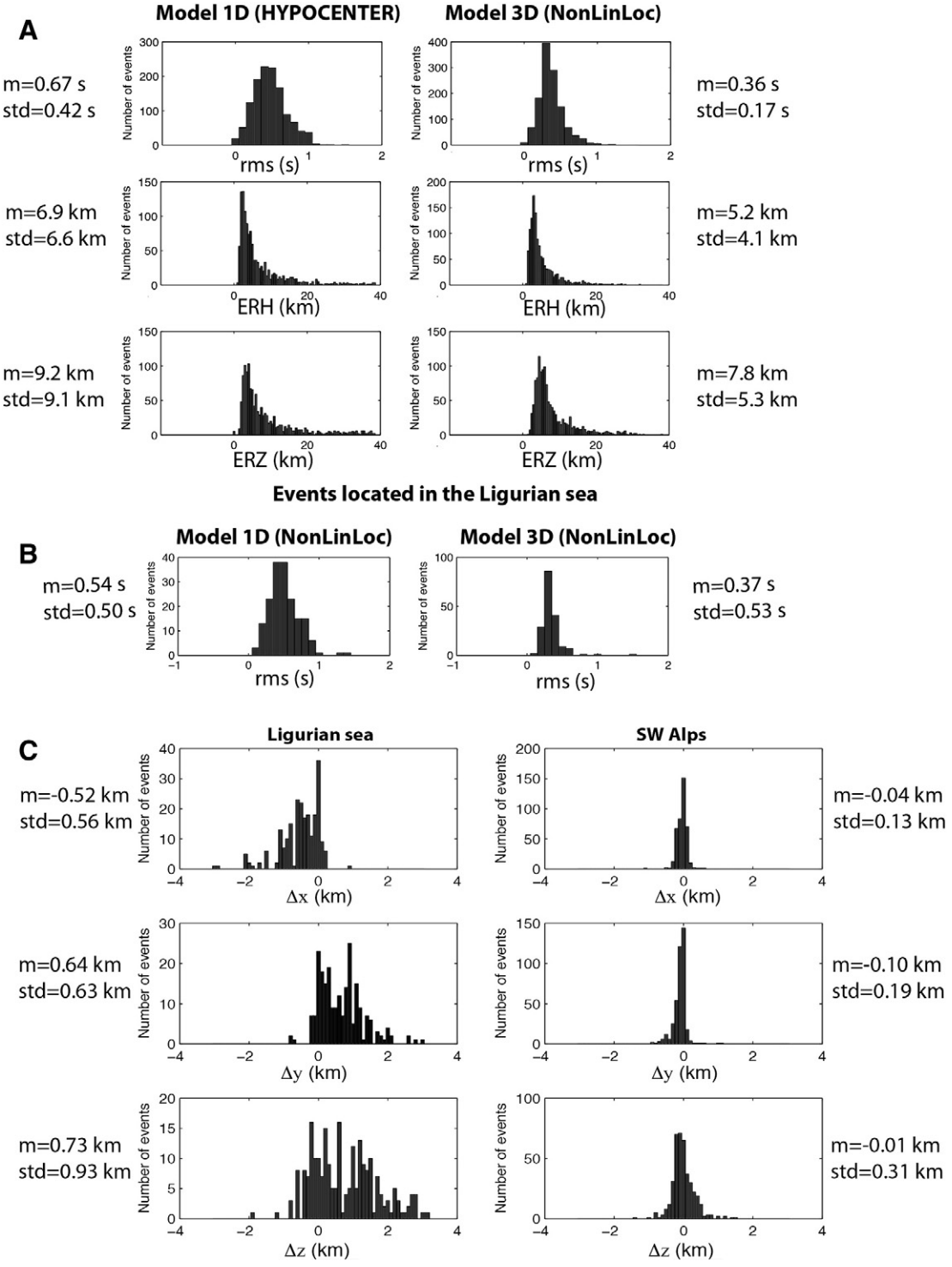

Fig. 5. a. Histograms of travel-time residual rms and uncertainties (dx, dy, dz) for the two location catalogues presented in Fig. 4: the first one from a 1D model code and the second one from a 3D model code. b. Histograms of travel-time residual rms for earthquakes located in the Ligurian sea, using NonLinLoc code. For the first one, the events are located with a "pseudo-code 3D" generated from the 1D model, for the second one the events are located with the 3D model. c. Histograms showing the location results of 3D synthetic P and S arrival-times simulated for earthquakes locations. Misfit of coordinates for earthquakes of the Southwestern Alps and of the Ligurian sea. For each histogram, the mean value and the standard deviation are indicated.

We first selected the period from January 2005 to December 2009. Then, we added the data from October 2000 to December 2001 corresponding to an earthquake swarm which occurred near Nice. We also added to the catalogue some events of magnitude larger than 3 which occurred in 2002, 2003 and 2004 and the 2011 seismic activity that occurred offshore Corsica, with a main shock of magnitude Mw = 4.9, in order to test the ability of our model to locate correctly events in the southernmost part of the study area, far outside of the seismic network.

4.2. Pre-location of events

In the frame of the SI-Hex project (Cara et al., 2015), we first carried out a 1D location for the 1500 events of our catalogue. We used the Hypocenter code (Lienert and Havskov, 1995), based on a linearized location method, and the 1D regional velocity model of Eva et al., 2001 (Table 1). By applying Wadati's methodology, we computed an average Vp/Vs ratio of 1.74, and checked that this model is consistent with our data set.

4.3. 3D earthquake location

Compared to 1D linearized methods, a direct search of earthquake locations has two main advantages: (i) it operates within realistic earth models which may have complicated 3D velocity variations; and (ii) it avoids problems of numerical convergence and of trade-offs between the determination of origin time and the inferred hypocentral depth. In order to test the stability of our results, we used two different approaches: the Maximum of Intersections method (Maxi) developed by Font et al. (2004), and improved by Theunissen et al. (2012), and the Non Linear Location method (NonLinLoc, Lomax and Curtis, 2001; Lomax et al., 2009).

Direct search location techniques pre-compute travel times from each seismic station to all nodes in the model and store them. In both these location techniques, the concept of equal differential time surfaces (EDT) is used (Zhou, 1994). A hyperbolic EDT surface includes all the velocity nodes of the model that satisfy the arrival time differences observed at two stations for a given earthquake. Theoretically, the hypocentre is located at the intersection of all available hyperbolic EDT surfaces resulting from the combination of all station pairs. However EDT volumes are to be defined corresponding to these EDT surfaces thickened by uncertainties parameters linked to the discretization of the velocity model as well as errors in velocity values and arrival times.

4.3.1. Maxi method

A table of propagation times for P and S waves was computed from each of the 180,000 nodes of the grid to the 56 stations available in our study area by using the shortest-path method (Moser, 1991).

To take into account uncertainties brought by errors defined above, a tolerance parameter TERR (in seconds) is chosen. The hypocentral solution corresponds to the intersection of EDT surface thickened by +/− the TERR value. Therefore, the hypocentre determination strongly depends on this value. The procedure to iterate this parameter in Maxi is detailed in Theunissen et al. (2012). In the present study, we made several runs with TERR varying between 0.4 s and 0.8 s with a 0.1-s step. In a first step, preliminary determination nodes (PRED), defined as nodes included in the maximum number of EDT volumes, were selected to target the volume in which the hypocentre will be searched. Starting from the PRED positions, travel time residuals are computed and inconsistent arrival times are removed. Then new PRED positions are computed corresponding to each TERR value. The procedure to obtain the final volume defining the hypocentre location is explained in Font et al. (2004) and Theunissen et al. (2012).

The confidence level of the solution is provided by the QEDT and D13 output parameters. The QEDT parameter is the ratio between the number of EDT volumes actually intersecting the solution and the number of EDT volumes initially constructed from the set of arrival times. The D13 parameter is the distance between two solution volumes defined before and after cleaning up for the outliers. Both parameters are indicative of the coherency between arrival times, the velocity model and the solution. The a-posteriori RMS and confidence axis are also computed (Font et al., 2004; Theunissen et al., 2012).

Table 1
1D model used for the preliminary locations.

Depth of the layer (km)	P wave velocity (km/s)
0	4.99
1	5.71
3	5.77
5	6.04
10	6.10
25	7.50
32	7.79
40	8.11

4.3.2. NonLinloc method

As in Maxi, a table of propagation times for P and S waves was computed from each of the 180 000 grid nodes to the 56 stations. Those travel times are computed with the eikonal finite difference scheme of Podvin and Leconte (1991).

NonLinloc uses efficient global sampling algorithms to obtain the a-posteriori probability density functions (PDF) over possible solutions. This location PDF quantifies the agreement between predicted and observed arrival times in relation to all uncertainties and forms a complete probabilistic solution. The NonLinloc software makes available two different likelihood functions to build the PDF. The first function incorporates the least square L2 norm, the second function, used in this study is based in the EDT formulation. The hypocentral solution including location uncertainties shown by density scatter plots is then computed by applying an Oct-Tree importance sampling (see Lomax and Curtis, 2001, for details).

NonLinLoc also provides the 68% confidence ellipsoid (Lomax et al., 2009), as well as the RMS value.

5. Results

5.1. General pattern

The distribution of epicentres (Fig. 2) corresponds, in broad approximation, to bibliographic results summarized below. The Mw magnitudes were computed using the approach followed by Cara et al. (2015).

In the north of the study area, numerous seismic events have been reported in the Ubaye region along the N140°E faults (Jenatton et al., 2007). Between the Argentera massif and the coast, the microseismic activity is documented on both N20°E and N140°E faults:

(1) the N140°E segments show right-lateral strike-slip fault activity (Madeddu and Béthoux, 1996; Eva et al., 1997; Sue et al., 1999; Turino et al., 2009);
(2) the N20°E direction corresponds to left-lateral faults, located just northeast of Nice (Courboulex et al., 2003).

Offshore, instrumental seismicity is characterized by low to moderate magnitude values, concerning mainly events located at the foot of the northern continental margin (Béthoux et al., 2008; Courboulex et al., 2003, 2007). Note that an Mw = 4.9 event surprisingly occurred in 2011 west of the Corsican margin where seismicity is usually very scarce. Focal mechanisms computed in the offshore domain indicate inverse faulting (Béthoux et al., 1992, 2008; Baroux et al., 2001). The same kind of mechanism is computed for the 2011 Corsican event (Larroque et al., submitted for publication).

Fig. 4 presents the distribution of seismicity at depth along three cross-sections. At the scale used here, earthquake positions resulting

from both 3D codes cannot be distinguished, and we present here the Maxi results. These 3D locations (black circles) can be compared to the 1D locations (white circles). Whatever the region considered, 3D locations are more clustered than 1D locations and the events located with the 1D model seem often deeper than the events located with the 3D model. In order to test the reliability of the depths obtained from the 3 locations, we added to our data set the arrival times of marine shots and quarry blasts. Their locations provide depths between −1 and 5 km, according to the quality of the data and available azimuthal coverage, whereas the corresponding 1D locations are sometimes more diffuse. In the next section results of synthetic process are shown in order to test the robustness of our 3D location methodology according to station distribution (and hence studied sub regions). Analyses on travel-time residual (rms) and uncertainties (dx, dy, dz) are also presented. Section 6 will focus on several sub-regions and discuss more quantitatively the shift between the different locations.

Profile (a) is a N–S cross-section along longitude 7.3° across the Ligurian Basin and the Argentera massif. There is almost no seismicity over the southern part of the Ligurian Basin, whereas we observe a few events in the western margin of Corsica, including the 2011 sequence, denoted in the map by a star. Some seismicity concentrates at the foot of the northern continental margin. In the first 15 km of the crust, we observe two almost vertical seismic clusters beneath the Argentera massif.

The E–W profile (b), along latitude 43.7° N, also shows how seismicity clusters under the continental margin and on land.

The E–W profile (c) corresponds to the northern limit of our model at 44.4°N. It crosscuts the edge of the external alpine zones, the Frontal Briançonnais Thrust (FBT) and the Penninic zone (P zone). The Ivrea body is shown as a green indentation in the crust. Several clusters can be observed. The westernmost ones are linked to the FBT. Towards the east, the Peninnic zone is also active. A dense cluster follows the boundaries of the Ivrea body, whereas a few deep foci are found along the edge of the Po plain. This distribution globally corresponds to that recorded during the GeoFrance 3D experiment (Paul et al., 2001).

5.2. Location uncertainties and accuracy

First, results of the whole catalogue have been compared in terms of associated errors (rms, dh, dz).

Fig. 5a shows the improvement in accuracy, when a 3D model is used with respect to the locations obtained with 1D model and the Hypocenter code. The average rms obtained is reduced from 0.67 s to 0.36 s and location uncertainties decrease also using 3D methodology with a greater dispersion of values for the 1D location results than using the 3D code. Note that a few location uncertainties are greater than 20 km. These results correspond to events associated with an important azimuthal gap and located far from the network.

The second test aims to evaluate the results obtained with the NonLinLoc code and a simple velocity model as the 1D model presented above. New travel times were processed from each seismic station to all nodes in this "pseudo 3D model" where the velocities are only function of the depth and the ratio Vp/Vs = 1.74, corresponding to our preliminary locations is used. The travel time residues are generally greater using this model than using the more realistic 3-D model. This is particularly true for the events occurring in the Ligurian Sea. In this case the ray path between the station and the oceanic crust is complicated and the resulting travel times are more realistic in the 3D model as shown in Fig. 5b.

We performed synthetic tests with the two targets. The first one is to show the robustness of location when the 3D model is used with respect to the 1D model described above. The second target is to evaluate the location uncertainties. We processed synthetic arrival times computed for two sets of initial events. The first one corresponding to favourable azimuthal coverage and the second one corresponding to events located far from the seismological events. We present in Fig. 5c the misfit between the true and relocated locations in the 3D model. For the events located around the Argentera massif the misfit of horizontal coordinates is limited to 100 m and the depth misfit mainly less than 500 m. For the events of the Ligurian Sea the results are more heterogeneous. The misfit of the horizontal coordinates is mainly less than 1.5 km. The misfit of longitudes is larger than the one of latitude. The depth misfit is more heterogeneous, generally less than 2 km but can reach 3 km. Note that this misfit is mainly positive, corresponding to retrieved hypocentres deeper than the initial ones. In the following we have to select the most constrained locations to avoid this trend.

At a larger scale than presented in Fig. 4, differences between Maxi and NonLinLoc results can be noted. In order to quantify and illustrate these discrepancies, we present in Table 2 the different locations obtained for some events, while Fig. 6 shows the corresponding error

Table 2
Comparison of locations obtained with different location codes.

				1 D			MAXI			NonLinLloc			REF			
Date	Hour	Mw	Lon °E	Lat °N	Depth	Lon °E	Lat °N	Depth	Lon °E	Lat °N	Depth	Lon °E	Lat °N	Depth	Ref
2000-11-26	04:41	3.0				7.60	44.016	2.4	7.621	44.020	2.5	**7.61**	**44.02**	**4.0**	Turino et al. (2009)
2000-12-19	00:52	2.9				7.350	43.787	0.5	7.354	43.786	3.2	**7.36**	**43.78**	**2.8**	Courboulex et al. (2003)
2000-12-19	14:20	3.2				7.365	43.782	1.5	7.361	43.786	3.2	**7.37**	**43.79**	**2.6**	Courboulex et al. (2003)
2000-12-20	05:45	3.0				7.356	43.783	4.6	7.365	43.795	0.4	**7.36**	**43.79**	**2.6**	Courboulex et al. (2003)
2000-12-21	06:35	2.4				7.361	43.781	1.1	7.363	43.790	1.7	**7.36**	**43.79**	**2.7**	Courboulex et al. (2003)
2001-02-06	22:28	4.1				8.609	44.128	5.0	8.650	44.092	3.2				
2001-02-25	18:34	4.6	7.516	43.494	15.1	7.457	43.526	12.8	7.452	43.542	13.7	**7.48**	**43.53**	**11.0***	Courboulex et al. (2003)
2001-02-25	18:53	2.1	7.526	43.502	19.8	7.465	43.512	14.1	7.459	43.515	13.7				
2001-02-25	20:33	3.5	7.476	43.52	16.7	7.450	43.555	18.0	7.447	43.539	18.1				
2001-05-30	17:37	2.5	7.132	44.147	7.2	7.111	44.128	9.0	7.118	44.136	7.9	**7.12**	**44.14**	**11.0***	Larroque et al. (2009)
2005-03-25	23:19	3.6				7.244	44.312	29.6	7.265	44.496	11.5	**7.296**	**44.490**	**10.9**	Sismalp
2005-12-20	23:57	3.3				6.944	44.104	3.5	6.944	44.105	0.6	**6.98**	**44.1**	**1.0***	Larroque et al. (2009)
2006-09-02	01:21	4.1				7.646	43.922	7.0	7.654	43.917	6.4	**7.64**	**43.91**	**7.1**	Turino et al. (2009)
2006-08-01	00:05	1.7				7.764	43.717	14.2	7.775	43.730	15.0				
2006-10-24	17:31	3.5				7.648	43.924	9.2	7.647	43.925	8.4	**7.62**	**43.91**	**9.0**	Turino et al. (2009)
2008-06-11	15:17	3.5	8.222	43.833	2.1	8.180	43.870	9.1	8.191	43.883	11.0	**8.156**	**43.869**	**14.2**	Dessa et al. (2011)
2008-10-24	03:06	4.1				7.320	44.369	11.3	7.306	44.382	10.1	**7.328**	**44.369**	**14.8**	Sismalp
2008-10-24	03:12	2.0				7.314	44.358	13.1	7.288	44.356	11.8	**7.282**	**44.361**	**10.4**	Sismalp
2011-07-02	14:43	4.0				7.603	41.932	10.1	7.673	41.984	9.6				
2011-07-07	19:21	4.9				7.600	41.935	13.8	7.658	41.977	13.3	**7.613**	**42.046**	**10.7***	Larroque et al. (submitted for publication)

In bold: reference to bibliographic results for some events (Courboulex et al., 2003; Larroque et al., 2009; Turino et al., 2009; Dessa et al., 2011; Larroque et al., submitted for publication).
The depths obtained by waveform inversion are denoted by a star.
For events occurring in the Ubaye region, the location available in Sismalp catalogue are chosen as reference due to the density of the Sismalp seismic network in the epicentral area.

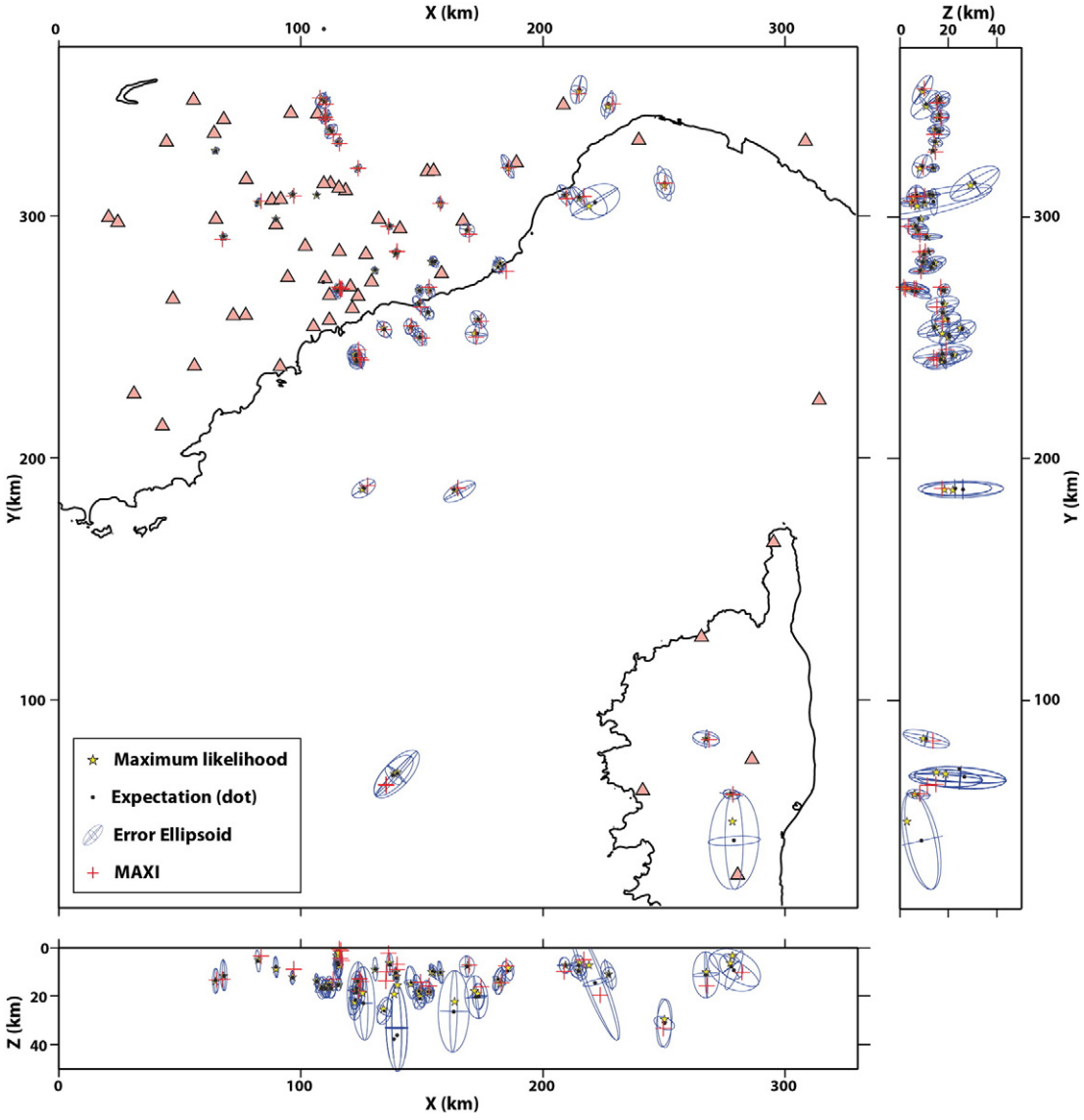

Fig. 6. For each histogram, the mean value and the standard deviation are indicated. Seismological stations within the model. Examples of locations obtained for the main events of the catalogue (largest magnitude) and some events already located in previous studies. Locations obtained with Maxi are denoted by red crosses. Expected locations obtained with NonLinLoc are dark dots and maximum likelihood locations are represented by stars. Error ellipsoids (68% level of confidence) as computed by the NonLinLoc code are superimposed.

ellipsoids computed by NonLinLoc. It is satisfying to observe that, for each earthquake, the error ellipsoid includes both locations (Maxi and NonLinLoc). Whereas these ellipsoids are very small within the seismic network, offshore, in the middle of the Ligurian Basin where seismicity is poorly monitored, their semi-major axes can reach 20 km. In the following, we mainly present NonLinLoc results because this code allows us to select easily the best constrained events: for geodynamical implications, we select only events where error ellipsoids have vertical axes shorter than 5 km for the inland part of the study area, and shorter than 10 km offshore.

In order to test the location stability when S arrivals are used, we also computed locations using only P arrivals. We observe, as already noted by Lomax et al. (2009), that one or more good-quality S readings better constrain the depth parameter. The efficiency of S arrival times is clearly demonstrated in the case of the seismic sequence of 25 February 2001, off Nice. In 2001 most stations were not yet equipped with broadband seismometers. Most signals were therefore saturated for the Mw = 4.6 mainshock, whereas S arrival times could be read for the Mw = 3.8 aftershock. Using the same stations but a reduced set of S arrival times, the error ellipsoid of the main shock happens—as could be anticipated—to be larger than that of the aftershock.

6. Comparison with published results

6.1. The Nice arc region

A dense seismological network has been installed over 6 months (from October 2000 up to April 2001) in the frontal part of the Nice arc (Courboulex et al., 2007). 348 micro-events, with magnitudes ranging from 0.1 to 3.4, were located in the centre of the network. The use of a multiplet technique revealed a very clear alignment of events in the N20 direction. The location of events and focal mechanisms show that two oblique segments of the so-called active Blausasc Fault (BF) were reactivated during this swarm-like activity (Fig. 7a and b). Fig. 7b shows a selection of these events as located by the permanent seismological network (at least 4 permanent stations), as well as by the temporary network. Events with magnitude larger than 2 are represented by larger circles. This limited activity contrasts with the quiescence of the

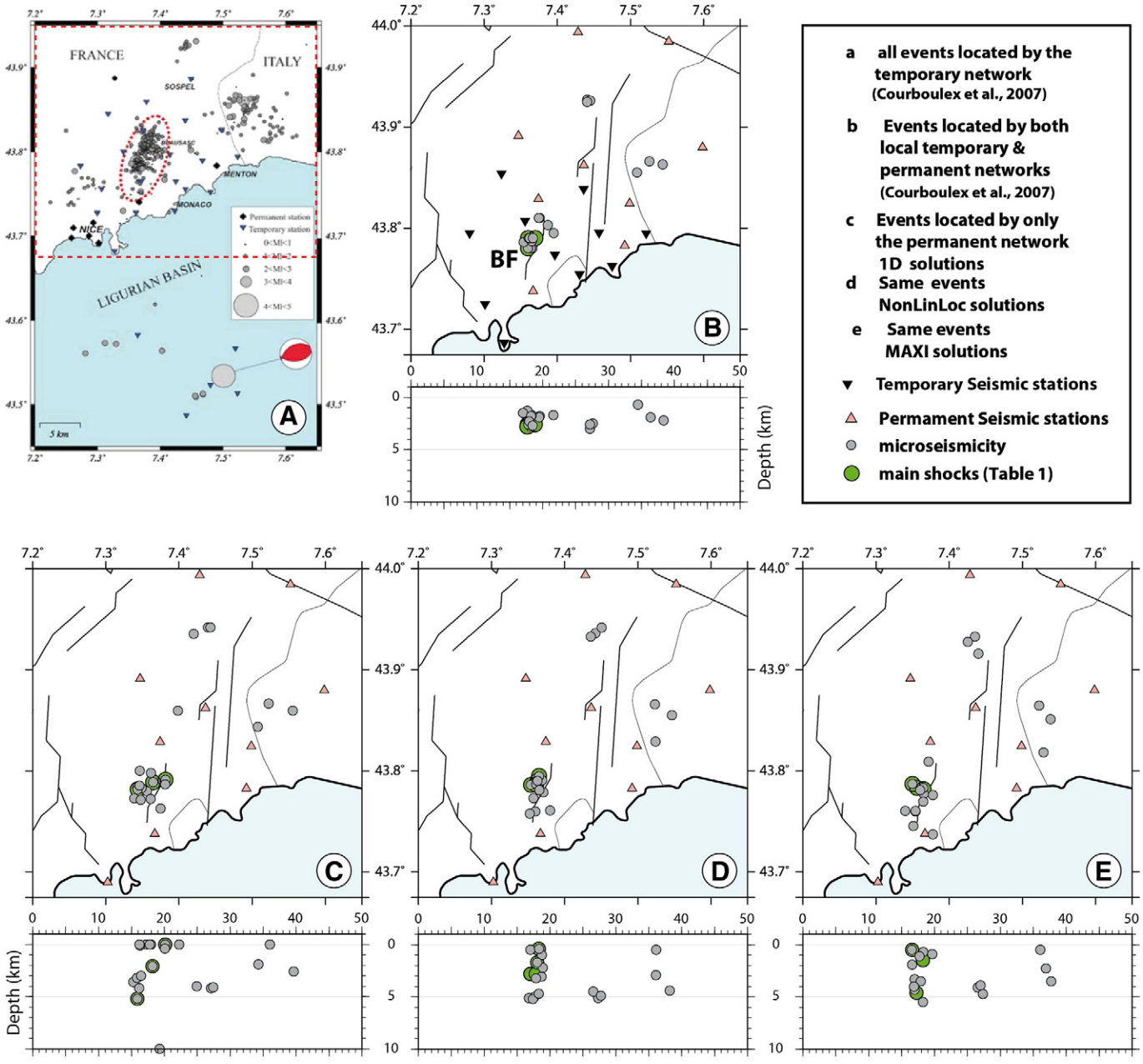

Fig. 7. Study of the 2000–2001 seismic activity near Nice. a. Local temporary network used and results obtained by Courboulex et al. (2007). b. Selection of events recorded by the permanent network as well as the local temporary network from Courboulex et al. (2007). BF: Blausac fault. c. 1D preliminary locations of these events using the permanent network only (see Fig. 5). d. 3D locations obtained with the NonLinLoc code. e. 3D locations obtained with the Maxi code.

fault observed in the time period 2005–2009, when only four small events of magnitude smaller than 2 were recorded by the permanent network. Fig. 7c to e compare locations obtained for the selected events of the 2000 sequence, using only a few permanent stations, farther from the epicentral area. Fig. 7c shows the 1D preliminary locations, Fig. 7d shows 3D locations obtained with the NonLinLoc code and Fig. 6e shows the locations obtained with MAXI code. Obviously, 3D locations do not cluster as tightly as multiplet locations of Fig. 7b. Table 2, which lists the different hypocentre positions for the main events, shows that the horizontal shift is about 1 km and the vertical shift about 2 km. For the smallest events, located with only 4 stations, errors are larger but compatible with the error ellipsoids computed by NonLinLoc (Fig. 6).

When we finally compare NonLinLoc locations to those obtained with the Maxi code (Fig. 7e), we observe that latter are also included in the NonLinLoc error ellipsoids (Fig. 6).

In this particular case the improvement brought by 3D location with respect to 1D location (obtained with the same network) is not notable, in contrast with other areas (Fig. 4).

6.2. The coast and North Ligurian margin

Assuming that some weak seismicity exists along faults which remain undetected by inland networks, some marine stations are necessary to address instrumental remoteness, to record and locate marine microseismicity, and to delineate active structures. This prompted the GROSMarin ("Grand Réseau d'Observation Sous-Marin") project, which consisted in a ~6-month deployment of an OBS array above the North Ligurian margin and the contiguous basin. The recording array was complemented by the installation of land mobile stations in order to densify the permanent network and to have homogeneous recording conditions over the whole instrumented area.

The seismicity detected during the recording period (April to October 2008) was rather low, constituting a set of 218 events. Moreover the strongest activity occurred in the northern part of the Argentera massif; hence, it was already detected by the permanent network. A few events were identified near the coast and at sea, mainly beneath the continental slope. The small events detected at sea by the GROSmarin network were not recorded by the permanent network. Fig. 8 shows the 1D locations for some events which occurred within the dense temporary land stations and OBS (Dessa et al., 2011), that can be compared with the 3D locations using only the permanent network. Here the discrepancy between Maxi and NonLinLoc code is very few and we choose to show only MAXI results. The horizontal shift is generally very small, whereas focal depths vary more significantly. Note that some events are of very small magnitude and are recorded by very few permanent stations only. The earthquake swarm located inland in Liguria occurred in July 2008; it included a shock of magnitude 2.8, and Scafidi et al. (2015) recognize this area as a zone of recurrent seismic activity. We conclude that in this case that location with a permanent network and a 3D model gives results as satisfying as locations with a dense temporary network and a 1D velocity model.

6.3. Saorge-Taggia Fault

Turino et al. (2009) computed precise locations for earthquakes that occurred in the vicinity of the Saorge Taggia fault (STF). The regional permanent networks were complemented by three temporary seismic stations to densify the network near the STF. The authors used the NonLinLoc code in a 3D model deduced from a regional tomography study. The 451 relocated events occurred in the 1986–2006 period. Only some events feature both in our catalogue and in theirs. The locations of some of them are listed in Table 2. Fig. 9a shows the 1D locations corresponding to our catalogue. Fig. 9b shows the 3D locations we

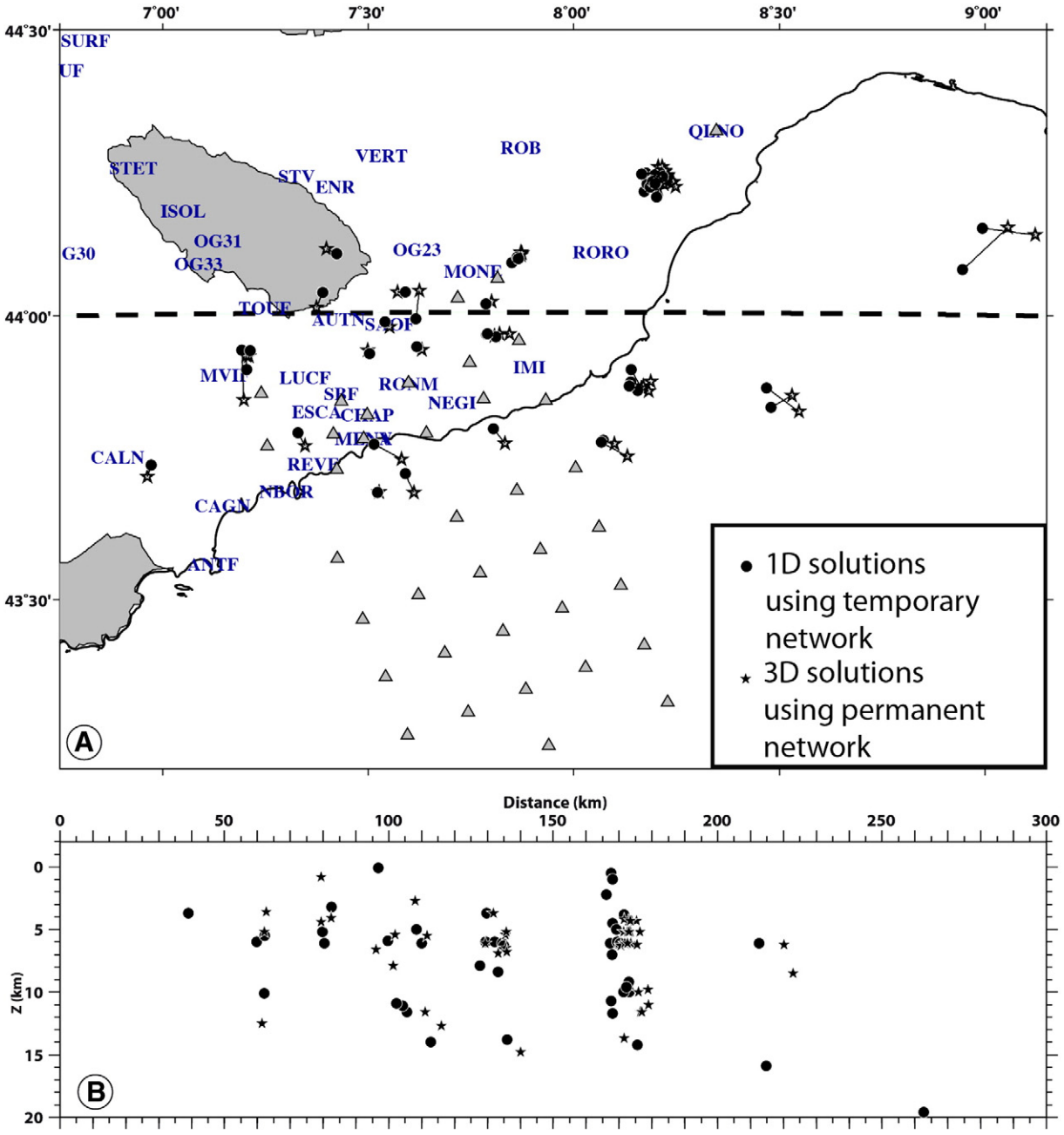

Fig. 8. GROSMarin experiment. Black dots: 1D locations obtained with the local temporary network (denoted by grey triangles); stars: 3D location obtained with the sole permanent network. Dash line shows vertical cross-section along the axis.

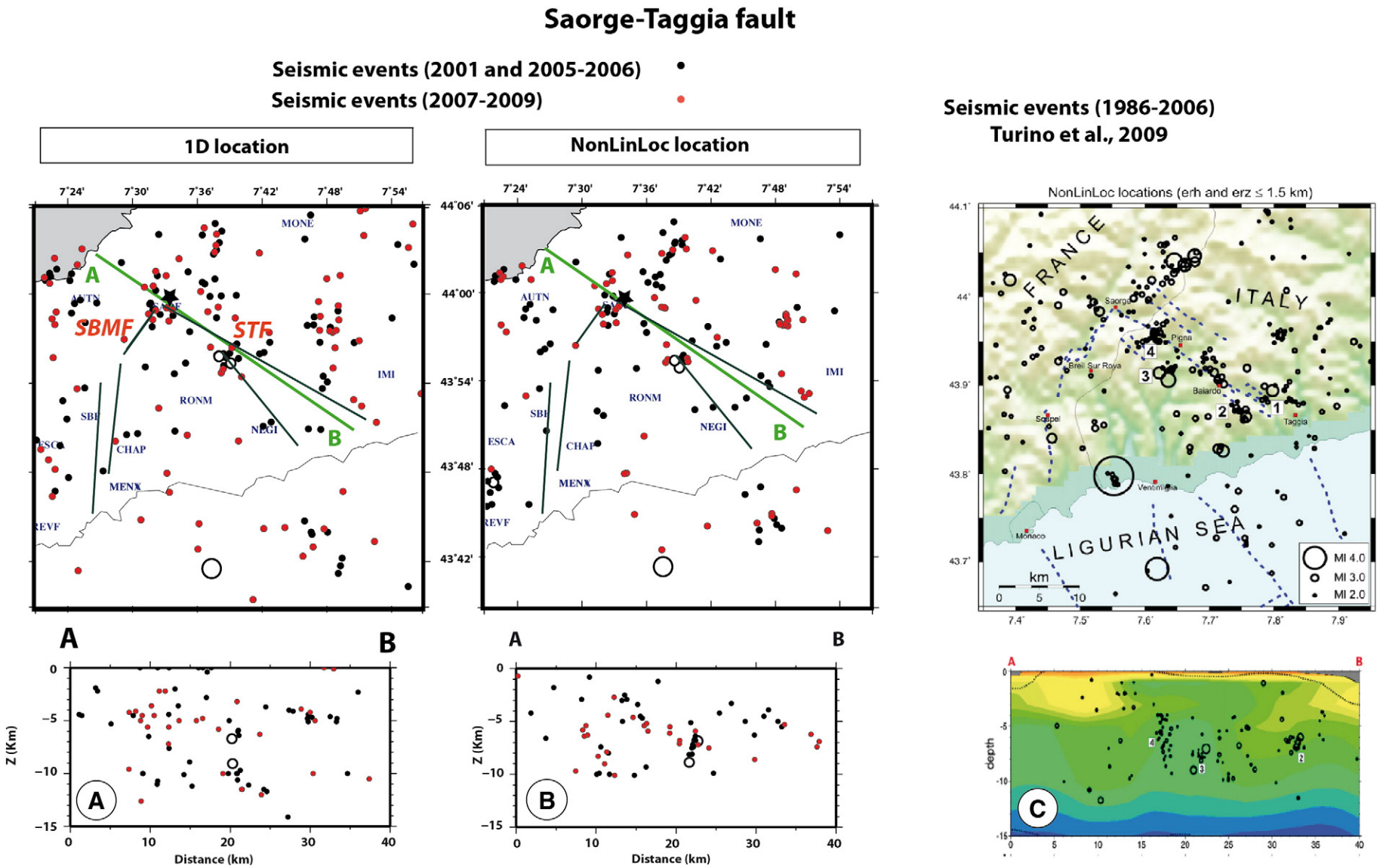

Fig. 9. Saorge-Taggia case study. a. 1D preliminary locations for events in our catalogue (2001 and 2005–2009). The Saorge-Taggia fault (STF) and the Saorge-Breil-Monaco fault (SBMF) are indicated. Cross-section along the AB axis is 5-km wide and parallel to the STF. b. 3D NonLinLoc locations and corresponding projections at depth. Events of largest magnitudes are denoted by white circles (see Table 2). c. Results from Turino et al. (2009) for the same area, but a different time period (1986–2006).

obtained with the NonLinloc code. These locations are clearly less scattered than those obtained in 1D, and they show some similarity with those of Turino et al. (2009) (Fig. 9c). Hypocentres are also drawn onto a cross-section along the STF. Turino et al. (2009) described the seismicity recorded near the STF and demonstrated that it is organized in small clusters, each cluster being active during a limited time period. More specifically, the 2006 seismic sequence is common to both catalogues (cluster 3 of Turino et al., 2009 in Fig. 9c). The seismicity from 2005 up to 2009 is also organized in clusters. Some of them differ from those of the previous time period (1996–2006) studied by Turino et al. (2009). In particular, we observed an earthquake swarm located at the connection between two faults: the Saorge-Breil-Monaco fault (SBMF) and the STF (Fig. 9). This area was already reactivated in 1983, with an Ml = 3.3 event, followed by numerous micro-earthquakes (Hoang Trong et al., 1987). Comparing our locations with those of Turino et al. (2009), we find the same kind of distribution at depth, as shown in the 10-km-wide cross-section along the STF: foci are located between 5 and 10 km at depth mainly along vertical alignments. It is worth noting the constant activity in time of the NE–SW alignment, that prolongates SMBF northeastward of the STF, which we interpret as the hidden prolongation of SBMF, already evidenced by Nicolas et al. (1998) and Turino et al. (2009). We discuss it in the next section.

7. The seismicity of the Argentera massif revisited

In Fig. 10 we observe that this microseismicity clusters along the N140° right-lateral system that runs along the south-western flank of the Argentera massif. This seismicity is located in the first 10 km of the crust). This seismicity is rather scarce and characterized by low-magnitude events. The recent SI-Hex catalogue (Cara et al., 2015), available for the whole instrumental period (1962–2009) and providing revised magnitudes Mw, shows that very low energy has been dissipated in the area during this time frame (Fig. 10). Only a few events have magnitudes larger than 3. We also included the 2 September 1982 event, studied by Bertil et al. (1989) and located near the village of Roquebillière, with a focal depth of 3.5 km, a normal faulting mechanism and a magnitude Ml = 3.2 revised as Mw = 2.9.

On the other hand, Sanchez et al. (2010) demonstrated that the area has been subject to deformation since at least the Holocene, as evidenced by offsets in glacial geomorphological surfaces. Using several pieces of evidence, they claim that this deformation is mainly accommodated by the >100-km-long dextral segmented “en échelon” system of the Jausiers–Tinée (JTF) and Sérennes–Bersezio (SBF) faults and conjugate minor N20 sinistral faults. In historical times, several earthquakes caused severe damage in an area ranging from villages located south of the Argentera massif (from Roquebillière to Saint-Martin-Vésubie) and as far as the coastal zone. Events in 1348, 1494, 1618, 1644, and chiefly the so-called Roquebillière event in 1564 are attested in historical archives (Lambert and Levret, 1996; Scotti et al., 2007) and tentatively located near Roquebillière in historical catalogues due to heavy damage reported in this village. Analyses of sediments in the lake of Vens and dating of homogeneous interbedded deposits (Petersen et al., 2014) confirm the occurrence of these historical earthquakes, with an approximate recurrence period of 600 years. Important site effects can partly explain the destructions described in historical archives. Nevertheless, the occurrence of major events to the south-west of the Argentera massif is attested even if the identification of rupture areas remains very speculative.

Our results allow to obtain less diffuse the repartition of the hypocentres in the area studied respect to the usual images a microseismicity in the region (see for instance, Larroque et al., 2009). The present-day microseismic activity relocated in this study confirms the segmentation of the major NW-SE faults (JTF and SBF), as already shown by tectonic field works (Sanchez et al., 2010). For these authors, the SBF and the JTF represent an active fault system which localizes most of the deformation in the area. The low deformation rate recognized in the South Alpine region is accommodated by numerous events of moderate magnitude in the Ubaye earthquake swarm, to the north-west of the Argentera massif (Jenatton et al., 2007; Daniel et al., 2011; Leclère et al., 2012), or in the Sampeyre earthquake swarm, to the north-east of our study area (Godano et al., 2013; Barani et al., 2014). This seismic activity would be favoured by a highly-fractured medium where fluids can progress and cause high pore pressure down to the seismogenic zone, at a depth of 5 to 10 km. Towards the south, this deformation is partially accommodated by creeping along the SBF and the JTF faults. The segmentation and rheological contrasts along inherited faults can favour slow stress and strain accumulation during long periods of time and occurrence of seismic ruptures at historical scale. The focal mechanism computed by Turino et al. (2009) along the ‘hidden’ NE–SW fault, close to STF, previously described and other mechanisms (Bauve et al., 2014) reveal thrust faulting south-east of the Argentera massif, whereas the JTF and SBF are transtensional faults. This change in tectonic regime exhibits a zone of shortening context where stress can concentrate (Manighetti et al., 2005; Mazabraud et al., 2013). Because an earthquake would more likely initiate at some high-stress spot, commonly an intersection zone between two oblique faults, we suggest that historical seismic events in the Vésubie valley occurred along a shallow rupture area situated just south of the Argentera massif. This rupture could connect there with the zone of N140–N20-striking faulting that continues east of the STF along the hidden fault discussed above. This location would better explain damage reported near the coast and site effects documented in the Argentera valley; it would also be consistent with the shallow instrumental seismicity (less than 10 km as computed in this study) observed at the south-eastern end of the cross-section AB (Fig. 10).

8. The seismicity of the Ligurian Sea revisited

Fig. 11a shows the seismicity pattern along the coastline, the continental margin and the northern part of the Ligurian basin. Cross-section AB (Fig. 11b) shows that foci follow a regular trend at depth, from the basin up to the coast. A new result of this study is the presence of rather deep hypocentres in the central part of the basin, at a 20-km depth. Taking into account for the vertical errors computed for these events by NonLinLoc, and the trend evidenced by the synthetic tests, these events are likely located between 17 and 20 km depth. Some events would therefore be located under the Moho. The basin, formed during Oligocene (Réhault et al., 1984), has not yet reached its post-rift thermal equilibrium. Béthoux et al. (2008) computed the temperature pattern inside the basin, using the thermo-mechanical modelling of Chéry et al. (2001) and taking into account the geometry of the basin, the rheology of the 3 crustal types (continental, transitional and oceanic) evidenced by seismic experiments, as well as heat flow data. The computed isotherm 350 °C, corresponding to the limit of the brittle domain, is located beneath the Moho (as determined by seismic and gravimetric studies) at the centre of the basin (Fig. 12a). Seismic ruptures could therefore occur there, in the uppermost mantle, down to a ~17–20 km depth. They can be linked to the normal faults issued from the rifting phase and reactivated as reverse faults.

Epicentres mainly gather beneath the continental margin (Fig. 11a). Some events such as the Mw = 4.5 2001 event (Table 2 and Fig. 11c) are located along the foot of the margin, from Nice to the gulf of Genoa. The largest-magnitude event in our catalogue is the Corsican event of 2011-07-07. With a focal depth of 9 to 13 km, a depth range corresponding to the oceanic crust domain (see Table 2), it occurred off the western Corsican margin, where the seismic activity, very atypical as shown by Larroque et al. (submitted for publication), is also very low.

Fig. 12b displays results obtained by Larroque et al. (2012) for the 1887 Imperia earthquake: these authors locate its epicentre at the foot

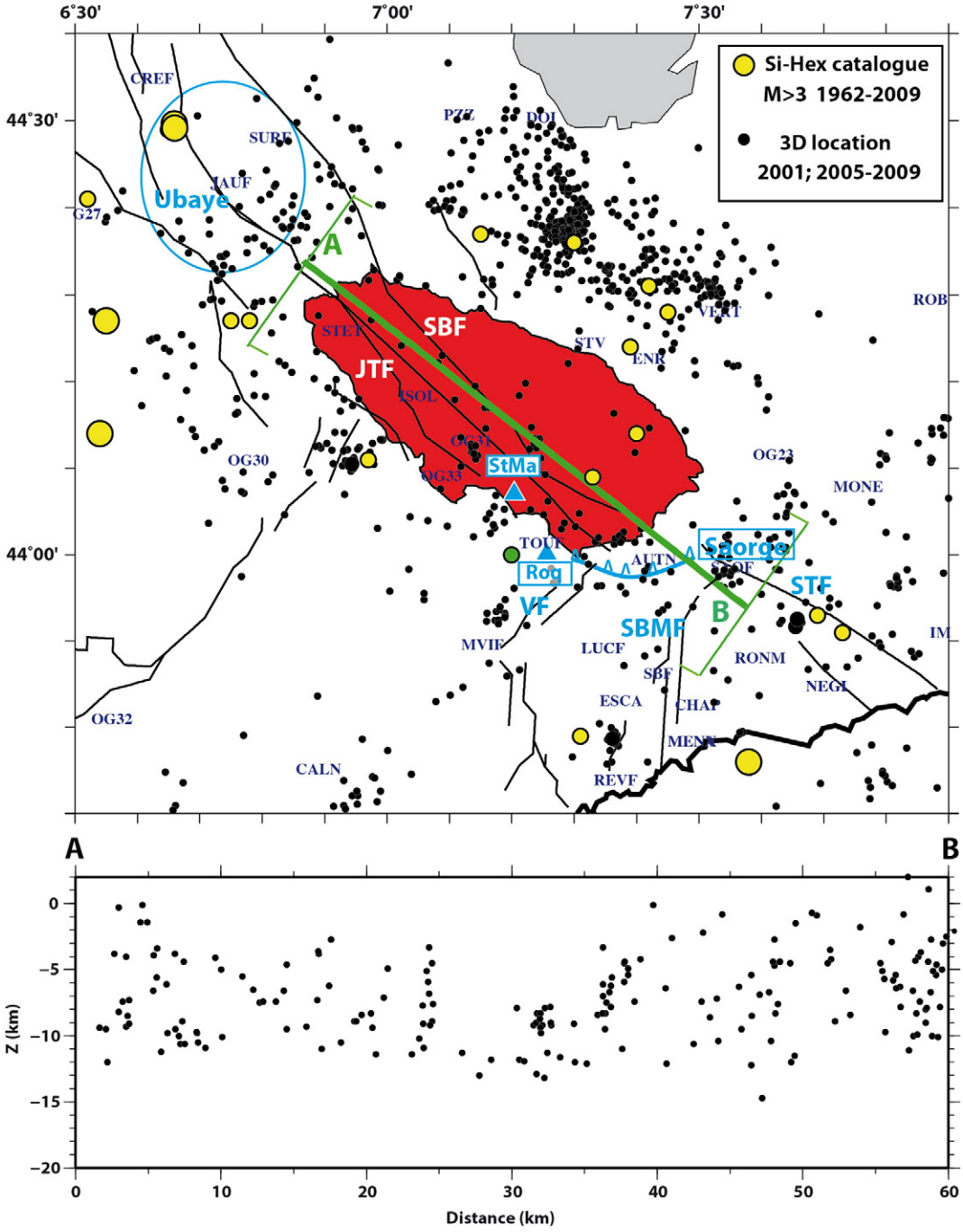

Fig. 10. Seismicity of the Argentera massif and surrounding regions. Contour of the massif is in red. Main faults, as indicated on tectonic maps (Bauve et al., 2014), identified by labels (SBF: Sérennes-Bersezio fault, JTF: Jausiers-Tinée fault, STF: Saorge-Taggia fault, SBMF: Saprge-Breil-Monaco fault, VF: Vésubie fault), as well as the Ubaye region. Two villages of the Vésubie valley (StMa = St Martin-Vésubie and Roq = Roquebillère) and Saorge village are located on the map. Seismic stations are also shown. The seismicity located in this study area is denoted by black dots whose size is proportional to the magnitude. Events of magnitude larger than 3 which occurred between 1962 and 2000 are superimposed (yellow dots). The 1982 event is denoted by a green dot. The dashed line A–B represents the location of the vertical, 20-km-wide cross-section shown under the map.

of the continental slope, off San Remo, at about 43.7°N and 7.8°E. It would have occurred along an inverse fault striking N55° and dipping at ~70° towards the south or, alternatively, at ~16° towards the north. We superimposed in Fig. 12b the 3D-located instrumental seismicity of the present study (colour dots). The location of these events is consistent with the extent of the Ligurian fault, as recognized at the foot of the margin by the recent MALISAR geophysical surveys (Larroque et al., 2012). Some events are located near the 1887 epicentre proposed by Larroque et al. (2012); others are closer to the coastline, regularly distributed, and parallel to the fault trace. For these events, focal depths are in good agreement with that inferred for the 1887 event (Larroque et al., 2012).

According to the tsunami modelling carried out by these authors, both reverse-faulting kinematics along north-dipping or south-dipping fault planes yield the same result for water movement. For the authors, the north dipping plane appears to be more likely geodynamically speaking. We have here too few well-constrained hypocentres to either confirm or contradict this view, let alone to provide independent estimate

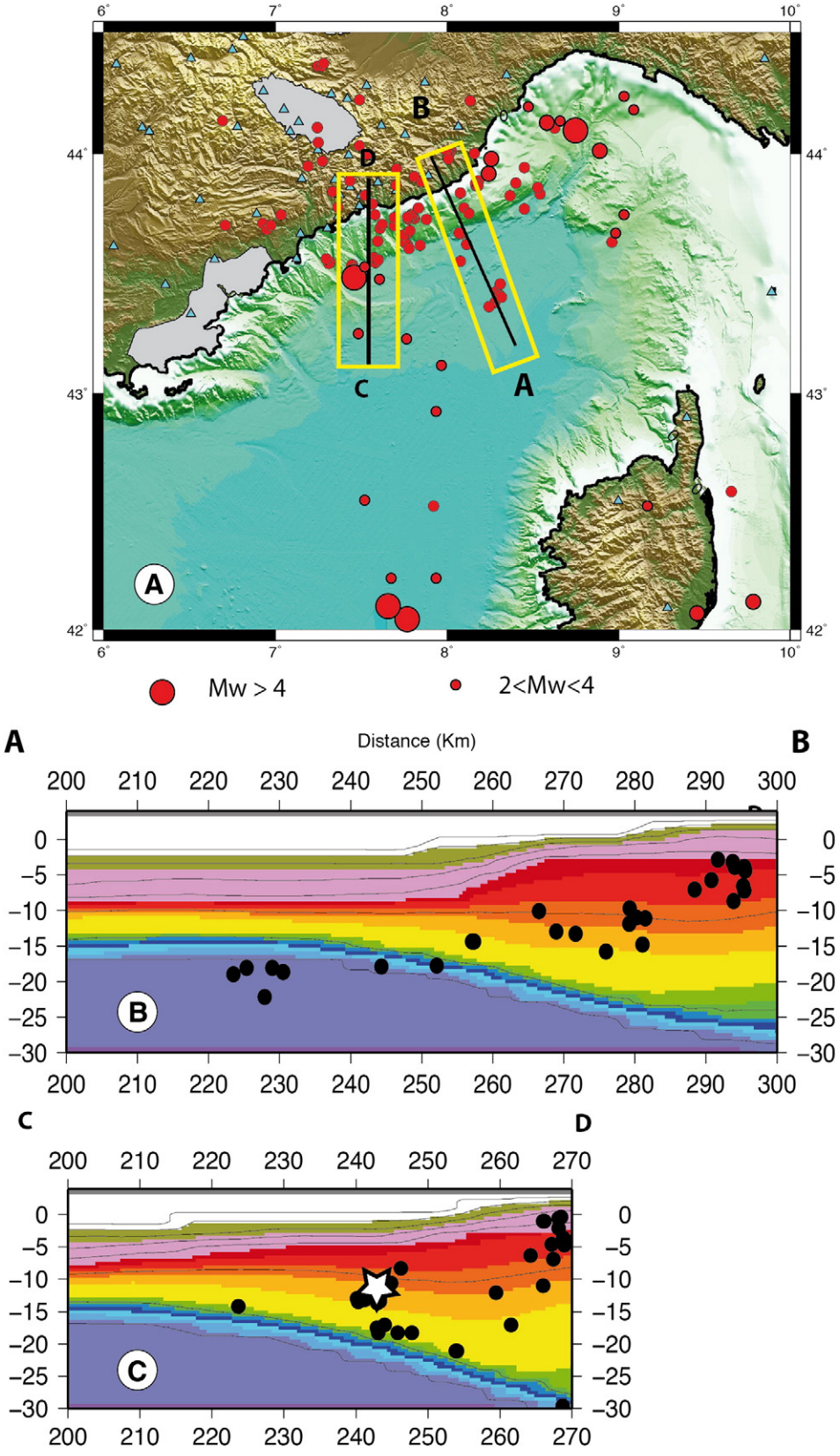

Fig. 11. a. Seismicity of the Ligurian Sea, superimposed on the topography-bathymetry map. Location of the 10-km-wide cross-sections through the seismicity located in the 3D model. b. Cross-section AB in the velocity model. c. Cross-section CD in the velocity model. The white star corresponds to the Mw = 4.5 2001 event.

of the fault's dip. Focal mechanisms computed for the larger events (Fig. 12b) confirm inverse faulting, but do not provide clear evidence about the dip of the nodal plane that would unambiguously correspond to the fault plane (Béthoux et al., 2008). Neither does the focal solution proposed by Courboulex et al. (2007) for the 2001 event, at the western end of the Ligurian fault system.

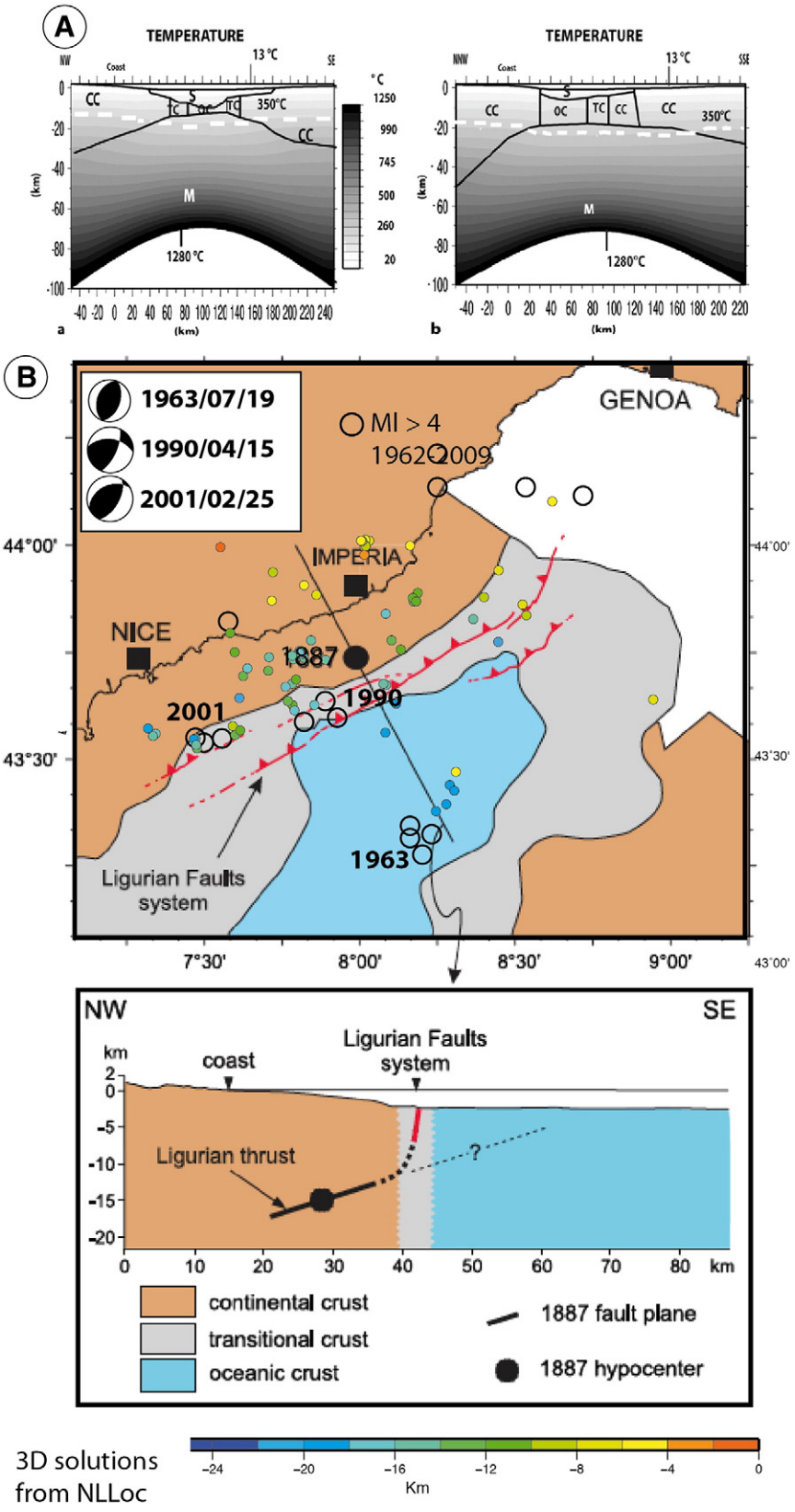

Fig. 12. a. Modelled temperature pattern in the Ligurian Sea, modified from Béthoux et al. (2008). Cross-section (a) is roughly located near cross-section CD of Fig. 10. Cross-section (b) is roughly located near cross-section AB of Fig. 10. b. Modified from Larroque et al. (2012), showing the location of the 1887 Imperia event. We superimposed the 3D-located seismicity of this study (colour dots). Empty circles are events with magnitude exceeding 4, recorded during the instrumental period (since 1962). Three bibliographic focal mechanisms are shown, taken from Béthoux et al. (1992) and Courboulex et al. (2007).

9. Conclusion

The first target of the paper was to describe the 3D structural model at the regional scale built from the Geomodeller process originally produced for geological and tectonic studies similar to those produced at smaller scale. We show that this model is also useful to constrain seismic event location.

In this study, we compared 1D locations with 3D locations for events distributed on a rather large region, from the Southwestern Alpine massifs up to southern Corsica through the Liguro-provençal oceanic domain. In this paper we focus on the methodology and on the different tests for determining the robustness and precision of our results. For epicentres inside the seismic network and close to the stations, results using 1D velocity model are very similar to 3D results. When events are located far from the stations and associated with an important azimuthal gap, the use of a 3D velocity model provides better results than 1D model locations. These 3D locations are particularly well adapted in the studied region characterized by very marked onshore/offshore transitions corresponding in depth to strong heterogeneities at the crustal and lithospheric scale. We recall that the Moho deepens to 50 km under the core of the southwestern Alps and is uplifted at the depth of 12.5 km at some parts of the basin.

In order to test the accuracy of our results we relocated quarry blasts and marine shots.

For the strongest events (Table 2) fine determinations of depth by waveform modelling are available (Courboulex et al., 2007; Larroque et al., 2009; Larroque et al., submitted for publication). The location in depth resulting from the 3D methodology is similar to these results.

If 1D locations are constrained for most of the strongest events, we show that the microseismicity distribution is more clustered using 3D model than using 1D model. Consequently, the 3D locations provide us a more accurate image of the global seismicity distribution in the South-Western Alps–Liguria region.

We showed, through a few examples dealing with small epicentral areas, that 3D locations using the permanent regional network are comparable to 1D locations using a dense temporary network surrounding the epicentre area. However the station coverage remains the key to well-constrained solutions whatever the model and the location code used.

We also confirmed that additional S arrivals improve the location and drastically reduces the location PDF, as already demonstrated by Lomax et al. (2009).

Both techniques used for location, Maxi and NonLinLoc, provide similar results when numerous data and/or good azimuthal coverage of stations are available. Where poor station distribution and large recording distances are met, as in the case of Corsica, hypocentres inferred from Maxi still fit within the ellipsoid volumes computed by NonLinLoc. The discrepancy between the two methods is in good agreement with uncertainties deduced from synthetic travel-time tests.

From a tectonic point of view, different seismic behaviours are evidenced in the Southwestern Alps. Some small faults—such as the Blausasc fault or the Peille-Laghet fault—are seldom (re)activated. Others—such as the Saorge-Taggia, the Tinée-Berzezio, the Jausiers-Tinée fault systems, or the fault in western Liguria responsible for the 2008 swarm (Scafidi et al., 2015)—are frequently visited by seismic clusters. It is worth noting that most of these clusters are characterized by low-magnitude events, which could be an evidence for weak coupling. Our 3D locations confirm that the seismogenic layer is shallow, generally in the 5–10-km depth range. The continuity of microseismic activity from the south of the Argentera massif towards a hidden fault located to the north-east of the Taggia fault leads us to hypothesize an epicentral zone for the 1564 earthquake, which remains the main seismic event in the region: it could have occurred between the small Vésubie fault and the area where two conjugate faults connect—namely the Saorge-Taggia and the Saorge-Breil-Monaco faults.

Compared to the south-western Alps, the Ligurian Sea presents a different behaviour. The instrumental seismicity recorded by the regional network seems rather scarce whereas we observed a few $M > 4$ events (two of them were relocated in this study). It is worth noting that the largest instrumental event which occurred in 1963 had a much higher magnitude ($Mw = 6$). The causes of stress amplification in this marginal basin are discussed in Béthoux et al. (2008). 3D-located hypocentres are clearly less scattered than when 1D location is used. Those revised locations shows hypocentres progressively deepening towards the centre of the basin; they also better agree with the geological structures. In particular, these locations tend to confirm the depth of the 1887 $Mw > 6.5$ earthquake, as estimated by Larroque et al. (2012). Despite rather large uncertainties, events located in the centre of the basin appear to have deeper foci than previously estimated and probably occur under the Moho.

In conclusion this work allows to present some improvement concerning the seismogenic depth determination and geometry of a few active faults respect to the numerous published studies dealing to the region, these parameters being of main importance in terms of seismic hazard assessment.

We studied here only a rather short time window of seismicity. Because locations presented in this study seem reliable, the same methodology could be applied to a larger seismic data catalogue in order to confirm these first results. Some improvement is also in progress to define a more accurate 3D velocity model.

Acknowledgements

This work was partly supported by SI-HEX project with financial support from the MEEDDM French Ministry (Convention MEEDDM-CNRS 007147).

We warmly thank Olivier Sardou for completion of the MNT from bathymetric and topographic data, Nincolas Chamot-Rooke, Tobias Diehl, Anne Paul, Davide Scafidi and Stefano Solarino for providing the numerical data of their gravimetry or tomography studies, and Dimitri Schreiber for the help in completion of the interface model in the 3D Geomodeller.

For their contribution to this work, we also acknowledge Yann Rolland and Anne Deschamps for fruitful discussions.

We are very grateful to Antony Lomax for his help in NonLinLoc code processing.

This paper was much improved by comments from Jean-Philippe Avouac and an anonymous reviewer.

References

Ansorge, J., Blundell, D., Mueller, S., 1992. Europe's lithosphere — seismic structure. In: Blundell, D., Freeman, R., Mueller, S. (Eds.), A Continent Revealed, The European Geotraverse. Cambridge University Press, pp. 33–69.

Barani, S., Ferretti, G., Scafidi, D., Spallarossa, D., 2014. Analysis of seismicity and microseismicity associated with the October–November 2010 Sampeyre swarm, Southwestern Alps. Tectonophysics 611, 130–140.

Baroux, E., Béthoux, N., Bellier, O., 2001. The state of stress of the southeastern France determined by seismological focal mechanisms inversion. Geophys. Int. 145, 336–348.

Bauve, V., Plateaux, R., Rolland, Y., Sanchez, G., Béthoux, N., Delouis, B., Darnault, R., 2014. Neogene to present-day stress fields feature transcurrent tectonics in the SW Alps. Tectonophysics 621, 85–100.

Bertil, D., Béthoux, N., Campillo, M., Massinon, B., 1989. Modeling crustal phases in southeast France for focal depth determination. Earth Planet Sci. Lett. 95, 341–358.

Bertrand, E., Deschamps, A., 2000. Lithospheric structure of the southern French Alps inferred from broadband analysis. Phys. Earth Planet. Inter. 122, 79–102.

Béthoux, N., Fréchet, J., Guyoton, F., Thouvenot, F., Cattaneo, M., Eva, C., Nicolas, M., Granet, M., Feignier, B., 1992. A closing Ligurian Sea? Pure Appl. Geophys. 139, 179–194.

Béthoux, N., Deschamps, A., Nolet, G., Bertrand, E., Contrucci, I., Sosson, M., Ferrandini, J., 1999. The deep structure of Corsica as inferred by a Broad Band seismological profile. Geophys. Res. Lett. 26 (17), 2661–2664.

Béthoux, N., Tric, E., Chéry, J., Beslier, M.-O., 2008. Why is the Ligurian Sea (Mediterranean sea) seismogenic? A thermo-mechanical modeling of a reactivated passive margin. Tectonics 27. http://dx.doi.org/10.1029/2007TC002232 (TC 5011).

Bigot-, C.F., Sage, F., Sosson, M., Deverchère, J., Ferrandini, J., Guennoc, P., Popoff, M., Stéphan, J.-F., 2004. Déformation pliocène de la marge nord-Ligure.„Les consequences d'un chevauchement cristal sud-alpin. Bull. Soc. Geol. Fr. 173 (2), 197–211. http://dx.doi.org/10.2113/175.2.197.

Calcagno, P., Chiles, J.P., Courrioux, G., Guillen, A., 2008. Geological modelling from field data and geological knowledge. Part I: modelling method coupling 3D potential field interpolation and geological rules. Inter. Phys. Earth Planet 171, 147–157.

Cara, M., Cansi, Y., Schlupp, A., et al., 2015. Si-Hex: a new catalog of instrumental seismicity for metropolitan France. Bull. Soc. Geol. Fr. 186 (1), 3–19.

Chamot-Rooke, N., Gaulier, J.M., Jestin, F., 1999. Constraints on Moho depth and crustal thickness in the Liguro-Provençal basin from 3D gravity inversion: geodynamic implications. In: DURAND, B., et al., Eds., The Mediterranean Basins: Tertiary Extension within the Alpine Orogen.-. Geol. Soc. Lond. Spec. Publ. 156, 37–62.

Chéry, J., Zoback, M.D., Hassani, R., 2001. An integrated mechanical model of the San Andreas fault in central and northern California. J. Geophys. Res. 106, 22,051–222066. http://dx.doi.org/10.1029/2001JB000382.

Contrucci, I., Nercessian, A., Béthoux, N., Mauffret, A., Pascal, G., 2001. A Ligurian (western Mediterranean Sea) geophysical transect revisited. Geophys. J. Int. 146, 74–97.

Contrucci, I., Mauffret, A., Brunet, C., Nercessian, A., Béthoux, N., Ferrandini, J., 2005. Deep structures of the northern Tyrrhenian sea from multichannel seismic profiles and on land wide angle refection/refraction seismic recordings (LISA cruse): geodynamic implications. Tectonophysics 406 (3), 141–163.

Courboulex, F., Larroque, C., Deschamps, A., Gélis, C., Charreau, J., Stéphan, J.F., 2003. An unknown active fault revealed by microseismicity in the south-east of France. Geophys. Res. Lett. 30 (15), 1782. http://dx.doi.org/10.1029/2003GL017171.

Courboulex, F., Larroque, C., Deschamps, A., Kohrs-Sansorny, C., Gélis, C., Got, J.L., Charreau, J., Stéphan, J.F., Béthoux, N., Virieux, J., Brunel, D., Maron, C., Duval, A.M., Perez, J.-L., Mondielli, P., 2007. Seismic hazard on the French Riviera: observations, interpretations and simulations. Geophys. J. Int. 170 (1), 387–400. http://dx.doi.org/10.1111/j.1365-246X.2007.03456.x.

Daniel, G., Prono, E., Renard, F., Thouvenot, F., Hainzl, S., Marsan, D., Helmstetter, A., Traversa, P., Got, J.-L., Jenatton, L., Guiguet, R., 2011. Changes in effective stress during the 2003–2004 Ubaye seismic swarm, France. J. Geophys. Res. 119, B01309. http://dx.doi.org/10.1029/2010JB007551.

Dessa, J.-X., Simon, S., Lelièvre, M., Beslier, M.-O., Deschamps, A., Béthoux, N., Solarino, S., Sage, F., Eva, E., Ferretti, G., Bellier, O., Eva, C., 2011. The GrosMarin Experiment: three dimensional crustal structure of the North Ligurian margin from refraction tomography and preliminary analysis of microseismic measurements. Bull. Soc. Geol. Fr. i182 (4), 305–321.

Diehl, T., Husen, S., Kissling, E., Deichmann, N., 2009. High resolution 3-D P-wave model of the Alpine crust. Geophys. J. Int. 179, 1133–1147.

Di Stefano, R., Kissling, E., Chiarabba, C., Amato, A., Giardini, D., 2009. Shallow subduction beneath Italy: three dimensional images of the Adriatic–European–Tyrrhenian lithosphere system based on high-quality P wave arrival times. J. Geophys. Res. 114, B05303.

Egger, A., Demartin, M., Andorge, J., Banda, E., Maistrello, M., 1988. The gross structure of the crust under Corsica and Sardenia. Tectonophysics 150 (3), 363–389.

Eva, E., Solarino, S., Eva, C., Neri, G., 1997. Stress tensor orientation derived from fault plane solutions in the southwestern Alps. J. Geophys. Res. 102 (B4), 8171–8185.

Eva, E., Solarino, S., Spallarossa, D., 2001. Seismicity and crustal structure beneath the Western Ligurian Sea derived from Local Earthquake Tomography. Tectonophysics 339, 495–510.

Font, Y., Kao, H., Lallemand, S., Liu, C.-S., Chiao, L.-Y., 2004. Hypocentral determination offshore Eastern Taiwan using the Maximum Intersection method. Geophys. J. Int. 158 (2), 655–675.

Gailler, A., Klingelhoefer, F., Olivet, J.L., Aslanian, D., 2009. Crustal structure of a young margin pair: new results across the Liguro-Provencal Basin from wide-angle seismic tomography. Earth Planet. Sci. Lett. 286 (1–2), 333–345.

Godano, M., Larroque, C., Bertrand, E., Courboulex, F., Deschamps, A., Salichon, J., Blaud-Guerry, C., Fourteau, L., Charlety, J., Deshayes, P., 2013. The October–November 2010 earthquake swarm near Sampeyre (Piedmont region, Italy): a complex multicluster sequence. Tectonophysics 608, 97–111.

Hirn, A., Sapin, M., 1976. La croûte terrestre sous la Corse: données sismiques. Bull. Soc. Geol. Fr. 18, 1195–1199.

Hoang Trong, P., Haessler, H., Holl, J.M., Legros, Y., 1987. L'essaim sismique (oct 1983–Janvier 1984) de la moyenne vallée de la Roya (Alpes Maritimes): activité récente d'un ancient système de failles conjuguées? CR Acad. Sci. Paris 304, 419–424.

Jenatton, L., Guiguet, R., Thouvenot, F., Daix, N., 2007. The 16,000 event 2003–2004 earthquake swarm in Ubaye (French Alps). J. Geophys. Res. 112, B11304. http://dx.doi.org/10.1029/2006JB004878.

Kissling, E., 1988. Geotomography with local earthquake data. Rev. Geophys. 26 (4), 659–698.

Lambert, J., Levret, A., 1996. Mille ans de séismes en France. Ouest Editions Presses Académiques, Nantes (120 pp).

Larroque, C., Béthoux, N., Calais, E., Courboulex, F., Deschamps, A., Déverchère, J., Stéphan, J.F., Ritz, J.F., Gilli, E., 2001. Active deformation at the junction between southern French Alps and Ligurian basin. Neth. J. Geosci. 80, 255–272.

Larroque, C., Delouis, B., Godel, B., Nocquet, J.-M., 2009. Active deformation at the south-western Alps–Ligurian basin junction (France–Italy boundary): evidence for recent change from compression to extension in the Argentera massif. Tectonophysics 467, 22–34. http://dx.doi.org/10.1016/j.tecto.2008.12.013.

Larroque, C., B. Delouis, F. Sage, M. Régnier, N. Béthoux, F. Courboulex, A. Deschamps, The 2011–2013 sequence of moderate earthquakes offshore western Corsica (western Mediterranean)., Tectonophysics. (submitted for publication)

Larroque, C., Scotti, O., Ioualalen, M., 2012. Reappreasal of the 1887 Ligurian earthquake (Western Mediterranean) from macroseismicity, active tectonics and tsunami modelling. Geophys. J. Int. http://dx.doi.org/10.11.11/13.65-246X.2012.05498x.

Laurent, O., Stéphan, J.-F., Popoff, M., 2000. Modalité et structuration miocène de la branche sud de l'arc de Castellane (chaines subalpines méridionales). Géol. Fr. 3, 33–65.

Leclère, H., Fabbri, O., Guillaume, D., Cappa, F., 2012. Reactivation of a strike-slip fault by fluid overpressuring in the southwestern French–Italian Alps. Geophys. J. Int. 189, 29–37.

Le Douaran, S., Burrus, J., Avedik, F., 1984. Deep structure of the north-western Mediterranean basin: result of two ship seismic survey. Mar. Geol. 55, 325–345.

Lienert, B.R.E., Havskov, J., 1995. A computer program for locating earthquakes both locally and globally. Seismol. Res. Lett. 66, 26–36.

Lomax, A., Curtis, A., 2001. Fast probabilistic earthquake location in 3D models using oct-tree importance sampling. Geophys. Res. Abstr. 3, 955.

Lomax, A., Michelini, A., Curtis, A., 2009. Earthquake location, direct global search methods. In Encyclopedia of Complexity and System Science. Part 5. Springer, New York, pp. 2449–2473.

Madeddu, B., Béthoux, N., Stephan, J.F., 1996. Déformations et champs de contraintes récents à actuel dans les Alpes sud-occidentales: approche sismotectonique. Bull. Soc. Geol. Fr. 167, 797–810.

Makris, J., Egloff, F., Nicolich, R., Rihm, R., 1999. Crustal structure from the Ligurian Sea to the Northern Apennines—a wide angle seismic transect. Tectonophysics 301, 305–319.

Manighetti, I., Campillo, M., Sammis, C., Mai, P.M., King, G., 2005. Evidence for self-similar, triangular slip distributions for earthquake and fault mechanics. J. Geophys. Res. 110, B05302.

Mazabraud, Y., Béthoux, N., Delouis, B., 2013. Is Earthquake activity along the French Atlantic margin favored by local rheological contrasts? C.R. Geosci. 345, 373–382.

Moser, T.J., 1991. Shortest path calculation of seismic rays. Geophysics 56 (1), 59–67.

Nicolas, M., Béthoux, N., Madeddu, B., 1998. Instrumental seismicity of the Western Alps: a revised catalogue. PAGEOPH 152 (4), 707–731.

Nocquet, J.M., Calais, E., 2003. Crustal velocity field of Western Europe from permanent GPS array solutions, 1996–2001. Geophys. J. Int. 154, 72–88.

Pascal, G., Mauffret, A., Patriat, P., 1993. The ocean-continent boundary in the Gulf of Lion from analysis of expanding spread profiles and gravity modelling. Geophys. J. Int. 113, 701–726.

Paul, A., Cattaneo, M., Thouvenot, F., Spallarossa, D., Béthoux, N., Fréchet, J., 2001. A three-dimensional crustal structure velocity model of the south-western Alps from local earthquake tomography. J. Geophys. Res. 106, 19367–19389.

Petersen, J., Wihelm, B., Revel, M., Rolland, Y., Crouzet, C., Arnault, F., Brisset, E., Chaumillon, E., Magand, D., 2014. Sediments of Lake Vens (SW European Alps, France) record large-magnitude earthquake events. J. Paleoclimatol. 51 (3), 343–355.

Podvin, P., Leconte, L., 1991. Finite difference computation of traveltimes in very contrasted velocity models: a massively parallel approach and its associated tools. Geophys. J. Int. 105, 271–284.

Réhault, J.-P., Boillot, G., Mauffret, A., 1984. The Western Mediterranean basin. Geological evolution. Mar. Geol. 55, 429–445.

Rollet, N., 1999. Structures profonde et dynamique du bassin ligure et de ses marges. Univ Paris VI, Thèse de Doctorat (293 p).

Rollet, N., Déverchère, J., Beslier, M.O., Guennoc, P., Réhault, J.P., Sosson, M., Truffert, C., 2002. Back arc extension, tectonic inheritance and volcanism in the Ligurian Sea, western Mediterranean. Tectonics 21, 3. http://dx.doi.org/10.1029/2001TC900027.

Sage, F., Beslier, M.O., Thinon, I., Larroque, C., Migeon, S., Angelier, J., Guennoc, P., Schreiber, D., Dessa, J.X., Michaud, F., Stéphan, J.F., Sonnette, L., 2011. Structure and evolution of a passive margin in a compressive environment: example of the south-western Alps–Ligurian basin junction. Mar. Pet. Geol. 28 (7), 1263–1282.

Sanchez, G., Rolland, Y., Schreiber, D., Corsini, M., Lardeaux, J.M., Giannerini, G., 2010. The active fault system of SW Alps. J. Geodyn. 49, 296–302.

Scafidi, D., Solarino, S., Eva, C., 2009. P wave seismic velocity and Vp/Vs ratio beneath the Italian Peninsula from local earthquake tomography. Tectonophysics 465, 1–23.

Scafidi, D., Barani, S., De Farrari, R., Feretti, G., Pasta, M., Pavan, M., Spallarossa, D., Turiono, C., 2015. Seismicity of North Western Italy during the last 30 years. J. Seismol. 19, 201–218.

Scotti, O., Larroque, C., Baumont, D., Virieux, J., Courboulex, F., Delouis, B., Deschamps, A., Vallee, M., Angelier, J., Béthoux, N., Bellier, O., 2007. Définition de scenarii sismiques pour la region de Nice. 7° Colloque National AFPS.

Schreiber, D., Lardeaux, J.M., Martelet, G., Courrioux, G., Guillen, A., 2010. 3D modelling of Alpine Mohos in South-western Alps. Geophys. J. Int. 180, 961–975.

Speranza, F., Chiappini, G., 2002. Thick skinned tectonics in the external Apennines, Italy: new evidence from magnetic anomaly analysis. J. Geophys. Res. 107 (B11), 2290.

Sue, C., Thouvenot, F., Fréchet, J., Tricart, P., 1999. Widespread extension in the core of the western Alps revealed by earthquake analysis. J. Geophys. Res: B Solid Earth and Planets 104, 25,611–25,622. http://dx.doi.org/10.1029/1999JB900249.

Theunissen, T., Font, Y., Lallemand, S., Gautier, S., 2012. Improvements of the maximum intersection method for 3D absolute earthquake locations. BSSA 102, 1764–1785 N° 4.

Thouvenot, F., Paul, A., Fréchet, J., Béthoux, N., Jenatton, L., Guiguet, R., 2007. Are there really superposed Moho in the south-western Alps? New seismic data from fan-profiling reflections. Geophys. J. Int. 170 (3), 1180–1194.

Tricart, P., Lardeaux, J.-M., Schwartz, S., Sue, C., 2006. The late extension in the inner western Alps: a synthesis along the south-Pelvoux transect. Bull. Soc. Geol. Fr. 177 (6), 299–310.

Turino, C., Scafidi, D., Eva, E., Solarino, S., 2009. Inferences of active faults at the Southern Alps–Liguria basin junction from accurate analysis of low energy seismicity. Tectonophysics 475, 470–479.

Vialon, P., Rochette, P., Ménard, G., 1989. Indentation and rotation in the western Alpine arc. Geol. Soc. Lond. Spec. Publ. 45, 329–338.

Waldhauser, F., Kissling, E., Mueller, S., 1998. Three-dimensional interface modelling with two-dimensional seismic data: the Alpine crust–mantle boundary. Geophys. J. Int. 135, 264–278.

Zhou, H.-W., 1994. Rapid three-dimensional hypocentral determination using a master station method. J. Geophys. Res. 99 (B8), 15 439–415 455.